Influence of transboundary transport of trace elements on mountain peat geochemistry (Sudetes, Central Europe)

Barbara Fialkiewicz-Koziel, Edyta Łokas, Mariusz Galka, Piotr Kolaczek, François de Vleeschouwer, Gaël Le Roux, Beata Smieja-Król

Quaternary Science Reviews 230 (2020) 106162

Contents lists available at ScienceDirect

Quaternary Science Reviews

journal homepage: www.elsevier.com/locate/quascirev

Influence of transboundary transport of trace elements on mountain peat geochemistry (Sudetes, Central Europe)

Barbara Fiałkiewicz-Kozieł [a, *], Edyta Łokas [b], Mariusz Gałka [c], Piotr Kołaczek [a], Francois De Vleeschouwer [d], Gael Le Roux [e], Beata Smieja-Król [f]

[a] Adam Mickiewicz University, Faculty of Geographical and Geological Sciences, Krygowskiego 10, Poznań, Poland
[b] Institute of Nuclear Physics, Polish Academy of Sciences, Radzikowskiego 152, 31-342, Kraków, Poland
[c] University of Lodz, Faculty of Biology and Environmental Protection, Department of Geobotany and Plant Ecology, Banacha 12/16, Lodz, Poland
[d] Instituto Franco-Argentino para el Estudio del Clima y sus Impactos (UMI IFAECI/CNRS-CONICET-UBA), Universidad de Buenos Aires, Intendente Guiraldes 2160, Ciudad Universitaria, Pabellon II - 2do. Piso, (C1428EGA) Ciudad Autonoma de Buenos Aires, Argentina
[e] EcoLab, Université de Toulouse, CNRS, INPT, UPS, Toulouse, France
[f] University of Silesia, Institute of Earth Sciences, Faculty of Natural Sciences, Będzińska 60, 41-200, Sosnowiec, Poland

ARTICLE INFO

Article history:
Received 19 July 2019
Received in revised form
14 November 2019
Accepted 1 January 2020
Available online 13 January 2020

Keywords:
Peat bog
Sources of pollution
Lead isotopes
REE
Uranium
Spheroidal aluminosilicates
Radionuclides
European black triangle

ABSTRACT

Mountain ombrotrophic peatlands in Central Europe are an important stock of transboundary contamination both of natural and anthropogenic origin. The Śnieżka Mountain (West Sudetes) forms a significant orographic barrier and receives aerosols from broadly-recognized anthropogenic sources (production and use of stainless steel, processing of uranium, coal combustion, nuclear weapon tests, and Chernobyl accident). The main objective of the study was to assess the pattern of distribution and origin of trace elements and to distinguish the long-range transport vs. local signals in two ^{210}Pb and ^{14}C – dated peat cores from the highest summit of the Karkonosze (West Sudetes) spanning the last 280 years.

Maximum values and accumulations of almost all investigated elements (Pb, Zn, Cu, Ni, Cr, Ti, Al, U, Sc, and REE) were identified around the 1970s. The analysis of peat using scanning electron microscopy (SEM) confirmed the occurrence of spheroidal aluminosilicate fly ash particles (SAP) in the topmost 40 cm (from AD 1938) together with a maximum of mullite ($3Al_2O_3 \cdot 2SiO_2$), an anthropogenic marker originating from coal-based power plants. The overall ^{206}Pb/^{207}Pb signature ranges from 1.160 to 1.173, indicating a predominant contribution of anthropogenic Pb. Human activities promote the release of mobile ^{234}U, due to the weaker bonds to mineral structure, and cause the radiogenic disequilibrium between ^{238}U and its daughter ^{234}U.

1. Introduction

Industrial activities caused dramatic changes in ecosystems, releasing uncontrolled amounts of trace elements influencing both biotic and abiotic components (Rose, 2015; Waters et al., 2016, 2018).

Atmospheric pollutants are transported by wind and dispersed at different geographical scales. The range of dispersion is dependent on the size of the particle and its chemical behaviour in the air (Samson, 1988). Larger particles are generally deposited close to the emitter (Samson, 1988) while regionally-recognized lighter particles can be transported from hundreds to thousands of kilometres, passing through cities, states, and countries, and strengthen the local pollution (Munn, 1972; Erel et al., 2002, 2006; Bergin et al., 2005). It results in a more global, uniform pollutant signal over continents for certain pollutants (i.e. contaminants carried by submicronic aerosols: artificial radionuclides, lead derived from the combustion of leaded gasoline).

Mountain ecosystems such as lakes and peatlands are sensitive archives of long-range transport (Arellano et al., 2011; Catalan et al., 2013; Le Roux et al., 2016; Okamoto and Tanimoto, 2016). Notwithstanding, the received input of dust depends on height above sea level (a.s.l.). The altitudes between 0 and ~2000 m a.s.l. are mainly subjected to vertical transport of Potentially Harmful Trace Elements (PHTE) (Le Roux et al., 2016). The free tropospheric zone, located above 2000 m a.s.l. is characterised by more lateral

* Corresponding author.
E-mail address: basiafk@amu.edu.pl (B. Fiałkiewicz-Kozieł).

https://doi.org/10.1016/j.quascirev.2020.106162

transport of PHTE (Catalan et al., 2013; Le Roux et al., 2016) and ecosystems located there receive dust mostly from long-range transport. The mutual effect of different climate factors like wind trajectories and precipitation play the most important role in mountain pollution (Catalan et al., 2013; Le Roux et al., 2016).

Peat bogs, exclusively fed by dry and wet atmospheric deposition, are significant biological filters and traps for PHTE and other elements. They give essential information about past and present changes in the environment, especially when applying a multiproxy approach (Lamentowicz et al., 2013; Gałka et al., 2019). Mountain peat bogs, located on plateaus, where the slope effect is minimal, are great archives of geochemical records of various origin (Le Roux et al., 2016).

The calculated accumulation of peat and, therefore, accumulations of elements enable to assess the past trends in pollution as well as to assess the sources of observed enrichments (e.g. Shotyk et al., 1998, 2002). REE elements are believed to be good indicators of lithogenic activity and natural sources of dust (e.g. Le Roux et al., 2012; Pratte et al., 2017; Vanneste et al., 2016), but they can also be indicators of anthropogenic activity (e.g. Fiałkiewicz-Kozieł et al., 2016).

The Sudetes (located at the border of Poland, the Czech Republic, and Germany) are an important region with long-time traditions of mining and ore processing (i.e. Fe, Cu, Pb, U, and Au) that may have had a great effect on PHTE deposited onto mountains. This mountain range is additionally surrounded by economically significant industrial centres and lignite-fired power plants, causing dramatic deterioration of environment in the 1970s and 1980s in Poland, the Czech Republic, and Germany. Due to dramatic environmental impact this area (e.g. Mazurski, 1986), named "Black Triangle" (BT), was qualified by the United Nations Environment Programme (UNEP) as an "ecological disaster zone" (Grübler, 2002; Kolář et al., 2015). Sparse investigations about mineralogy, pollen analysis, sulfur and carbon isotopes exist (i.e., Popowski, 2005; Skrzypek et al., 2009; Kajukało et al., 2016), but information about past PHTE contamination in peat bogs from the Sudetes is scarce (i.e. Strzyszcz and Magiera, 2001; Fiałkiewicz-Kozieł et al., 2015a). The most detailed anthropogenic signal in central Europe was estimated in the Czech Republic (i.e., Novak et al., 2003, 2008; Ettler et al., 2004; Ettler et al., 2006; Mihaljevič et al., 2006; Bohdálková et al., 2014). Only a few multiproxy studies including advanced geochemical analyses were carried out on peatlands from Poland (e.g. De Vleeschouwer et al., 2009; Fiałkiewicz-Kozieł et al., 2018).

Here we present a detailed multiproxy geochemical record from two cores of the Na Równi pod Śnieżką (NRS) peatland, located at the feet of the Śnieżka summit (1400 m a.s.l.), the highest mountain of the Sudetes. We hypothesised that long-range transport mainly contributes to the pollution of NRS. Our aims are: (1) to assess the pattern of distribution and origin of trace elements and REE (2) to distinguish the most significant signals of pollution in areas impacted by transboundary anthropogenic pollution and (3) to explain the fate of strategic elements like uranium after anthropogenically-driven release to the atmosphere.

2. Material and methods

2.1. Study site

The Sudetes are surrounded by industrial centres located in Poland (Lower Silesia) as well as in the Czech Republic (Northern Bohemia) and Germany (Saxony and Brandenburg). These three areas constitute the so-called Black Triangle (Fig. 1). In the 1970s and 1980s, the "Black Triangle" was one of the most polluted areas in Europe due to the uncontrolled density of factories and power plants, which, working without filters, released enormous amounts of alkali dust and toxic gases (mainly SO_2) in the atmosphere (Jędrysek et al., 2002; Szynkiewicz et al., 2008).

The Na Równi pod Śnieżką (NRS) peatland (50°44′18,31″N, 15°41′59,72″E) is located on a plateau (1350–1450 m a.s.l.) in the Karkonosze range, close to the highest summit of Mt Śnieżka (1602 m a.s.l.). The Karkonosze area is ~60 km long and up to 20 km wide granitic massif in the West Sudetes at the northern periphery of the Bohemian Massif, straddling the Czech/Polish border and forming the eastern extremity of the European Variscan belt (Mazur et al., 2006). The Karkonosze unit was lifted during Alpine orogeny, forming currently a steep rocky mountain range with numerous glacial landforms. Consequently, it is a significant orographic barrier for different types of air masses. During the 64% of the year, the area is directly influenced by the zonal circulation of oceanic air masses from the North Atlantic, flowing over the lowlands of Western Europe. 30% of the year is characterised by the influence of polar continental air masses, flowing from the east, 4%- by arctic air from the north and 2% - by tropical air masses, coming from the south (Sobik et al., 2014). The mean annual air temperature at Mt. Śnieżka is +0.5 °C and the annual precipitation ~1500 mm (Sobik et al., 2014; Migała et al., 2016). The dominated winds are the westerlies, amongst which SW and S winds dominated while NW and W are less frequent (Schwartz et al., 1994; Sobik et al., 2014, Fig. 1).

2.2. Coring and subsampling

Two cores of 63 and 67 cm long (Sn1 and Sn2, respectively), were retrieved in the spring of 2012 using a stainless steel 10 × 10 × 100 cm Wardenaar corer (Wardenaar, 1987). The distance between them was 20 m. Monoliths were wrapped in plastic bag, transported to the laboratory in Poznań (UAM), and stored in the laboratory cooler. Fresh cores were cut into 1-cm thick slices (except the top 6 cm, which were cut on 2 cm slices) using a carbon steel knife. Fresh cutting was necessary for detailed mineralogical analysis as freezing the peat core (as it is frequently done before slicing) would have caused a transformation of minerals by changing the temperature and water conditions of the catotelm. Protocols from Givelet et al. (2004) and De Vleeschouwer et al. (2010) were used to minimise contamination. Several geological samples such as the local rocks (granite, hornfels from Śnieżka), lignite coal (mine Turoszów), fly ash from Power Plant Turów, aircraft fuel (Laboratory Warter fuels, Płock, Poland) were also collected.

2.3. Ash content, bulk density, plant macrofossils

Dried bulk density was determined using fresh material collected with a 5-cm^3 beaker. Ash content (AC), used to quantify the relative proportion of mineral fraction in the peat, was determined by burning the dry samples at 550 °C overnight. High-resolution (1-cm peat slices) plant macrofossil analysis was used to reconstruct local ecological conditions and peat-forming plants in contiguous samples of approximately 20 cm^3 in the two profiles (comp. Suppl.1). The samples were washed and sieved under a warm water current over 0.2-mm mesh sieves. Vascular plants and brown mosses composition were determined on the basis of carpological remains and vegetative fragments (leaves, rootlets, epidermis) using the available identification keys (e.g. Smith, 2004; Mauquoy and van Geel, 2007). The identification of *Sphagnum* to species level was carried out separately on stem leaves using specific keys (Hölzer, 2010; Laine et al., 2011).

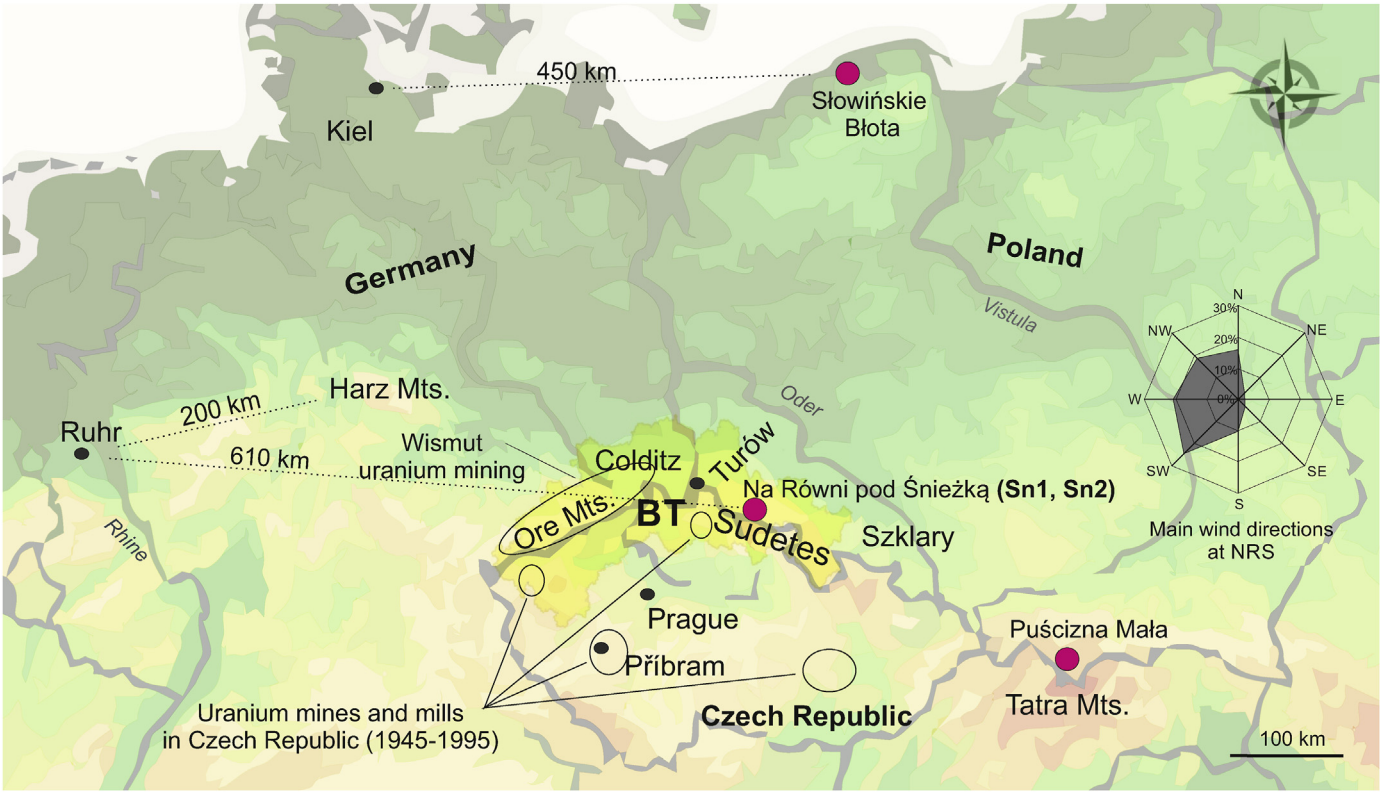

Fig. 1. Location of the study site (NRS) as well all places mentioned in the text. The wind rose (Sobik et al., 2014). The localisation of Wismut company (Wolkersdorfer, 1995), localisation of Czech uranium mines and mills (Cechák and Kluson, 2006), spotted line – the distance between the source of emission and destination, pink spot – investigated Polish peatlands, described in the text. (For interpretation of the references to colour in this figure legend, the reader is referred to the Web version of this article.)

2.4. Dating

The Sn1 profile was analyzed by gamma (^{137}Cs) and alpha (^{210}Po, ^{238}Pu, $^{239+240}$Pu, ^{234,238}U) spectrometry (comp. Table 1, Fig. 2). Separated slices were dried at 105 °C, homogenised, and taken for gamma spectrometric measurement. For ^{137}Cs analyses, samples were packed into 100 ml polypropylene cylindrical containers and were measured using high-resolution gamma spectrometry with a planar HPGe (high-purity germanium) detector with a composite foil window made of carbon fiber which support a capon foil covered with ultra-thin aluminum foil (homemade by Institute of Nuclear Physics PAS Krakow and electronics by Silena S.p.A.). A small amount of sample material was deposited on the bottom of the container. Activities of ^{137}Cs were determined via the ^{137m}Ba emission peak at 662 keV. Spectra were collected for 12–72 h, depending on the activity of the samples. The activities of ^{210}Po, ^{238}Pu, $^{239+240}$Pu, and ^{234,238}U were determined for about 1 g of dried samples. Samples were digested with radioactive tracers (^{208}Po, ^{242}Pu, ^{232}U) and a concentrated mixture of HNO_3, HCl, H_3BO_3, and H_2O_2 and slowly dried. Details of this procedure were described in previous articles (Mietelski et al., 2008; Łokas et al., 2013; Mróz et al., 2017). The activity of total ^{210}Pb was determined indirectly by measuring its decay product, ^{210}Po, using alpha spectrometry. ^{210}Po was chemically extracted from the material. Po isotopes were deposited on an Ag disc. Solution after polonium separation was used for Pu separation. Plutonium alpha sources were prepared by the NdF_3 microcoprecipitation method (Sill, 1987; Rao and Cooper, 1995). The effluent solution (8 M HNO_3) after Pu separation was used for U determination. Uranium was co-precipitated directly from this elution using NdF_3 and Mohr's Salt (ammonium iron sulfate) to obtain a thin spectrometric source (Łokas et al., 2010; Mietelski et al., 2016). Activity concentrations for polonium, plutonium, and uranium isotopes were determined using alpha spectrometers (Silena AlphaQuattro, Ortec Alpha Duo or Canberra 7401; all equipped with Canberra or Ortec ion-implanted silicon detectors). For this radiochemical procedure blank samples were made of reagents and were analyzed after each thirty sample. Alongside blanks and samples, the reference materials (IAEA Moss-Soil 447 and IAEA Sediment 385) were analyzed to ensure the quality of measurements. The obtained results: 447 (^{234}U- 20.8 ± 1.8; ^{238}U - 21.4 ± 2.2; ^{238}Pu - 0.14 ± 0.01; $^{239+240}$Pu - 4.96 ± 0.32, ^{210}Po - 415 ± 10; ^{137}Cs - 421 ± 22); 385 (234U- 27.9 ± 1.9; 238U - 29.4 ± 2.2; 238Pu - 0.40 ± 0.06; 239 + 240Pu - 2.70 ± 0.23) fall within 93–99% of certified values.

Seven samples from Sn1 and five samples from Sn2 were subjected to ^{14}C measurements in Radiocarbon Laboratory in Poznań. Hand-picked plant macrofossils, stored in MilliQ water, were selected for dating (Table 2). An absolute chronology is based on (i) the age-depth models calculated on ^{14}C dates in the OxCal v. 4.3 software (Bronk Ramsey, 1995) applying the IntCal13 (Reimer et al., 2013) and BOMB13NH1 (Hua et al., 2013) atmospheric curves as the calibration set and (ii) ^{210}Pb dates obtained for the section of 0–52 cm in the Sn-1 profile (Fig. 3). Additionally, patterns of SAP and mullite were used as chronomarkers and included in age-depth model for Sn2 (comp. Fiałkiewicz-Kozieł et al., 2016). For the calculation of the models based on ^{14}C dates, the *P_Sequence* command (Bronk Ramsey, 2008) with k parameters equal to 1 cm^{-1} and $log_{10}(k/k_0) = 1$ was applied. In the case of the Sn1 profile, the section between 0 and 52 cm, being dated using ^{210}Pb method (CRS model) (Table 1 and Fig. 2), was validated by ^{14}C dates. The CRS model assumes a constant rate of supply of unsupported ^{210}Pb to the peat surface despite variable sedimentation rates (Appleby and

Table 1
Activities of radionuclides measured in Sn1 profile.

Depth of middle layer (cm)	^{238}Pu (Bq/kg)	$^{239+240}$Pu (Bq/kg)	^{137}Cs (Bq/kg)	^{210}Pb unsupported (Bq/kg)	^{238}Pu (Bq/m^2)	$^{239+240}$Pu (Bq/m^2)	^{137}Cs (Bq/m^2)	^{210}Pb unsupported (Bq/m^2)
1.25	<0.06	<0.06	2255 ± 100	376 ± 29			2912 ± 135	486 ± 37
3.75	<0.06	<0.06	1286 ± 560	417 ± 47			1159 ± 500	376 ± 42
6.5	<0.04	<0.04	1018 ± 140	273 ± 41			685 ± 95	184 ± 27
9	<0.03	<0.03	878 ± 280	193 ± 25			235 ± 75	52 ± 7
10.5	<0.04	<0.04	789 ± 40	251 ± 36			171 ± 9	54 ± 8
11.5	<0.05	<0.05	486 ± 44	200 ± 26			266 ± 24	110 ± 14
12.5	<0.05	<0.05	406 ± 59	223 ± 12			211 ± 31	116 ± 6
13.5	<0.06	<0.06	469 ± 37	273 ± 18			223 ± 18	130 ± 9
14.5	<0.05	<0.05	321 ± 44	186 ± 24			126 ± 17	73 ± 9
15.5	<0.04	<0.04	429 ± 53	222 ± 30			166 ± 20	86 ± 11
16.5	<0.16	<0.16	365 ± 67	275 ± 46			152 ± 28	115 ± 19
17.5	<0.04	<0.04	163 ± 56	232 ± 31			67 ± 23	96 ± 13
18.5	<0.05	<0.05	206 ± 46	213 ± 23			84 ± 19	86 ± 9
19.5	<0.06	<0.06	377 ± 74	212 ± 28			185 ± 36	104 ± 14
20.5	<0.07	<0.07	328 ± 60	191 ± 22			138 ± 25	80 ± 9
21.5	<0.49	<0.49	193 ± 46	136 ± 10			99 ± 24	70 ± 5
22.5	<0.06	<0.06	172 ± 30	194 ± 25			87 ± 15	99 ± 13
23.5	<0.06	0.30 ± 0.07	1011 ± 48	246 ± 28		0.18 ± 0.04	604 ± 29	147 ± 17
24.5	<0.08	<0.08	465 ± 13	178 ± 25			256 ± 7	98 ± 14
25.5	<0.09	0.44 ± 0.08	368 ± 37	199 ± 18		0.30 ± 0.06	250 ± 25	135 ± 12
26.5	<0.04	0.48 ± 0.15	699 ± 58	101 ± 6		0.25 ± 0.07	359 ± 30	52 ± 3
27.5	<0.20	1.05 ± 0.18	286 ± 30	129 ± 19		0.61 ± 0.10	167 ± 18	75 ± 1
28.5	<0.09	1.32 ± 0.14	248 ± 46	186 ± 10		0.76 ± 0.08	144 ± 26	108 ± 6
29.5	0.45 ± 0.14	4.33 ± 0.64	165 ± 46	158 ± 12	0.25 ± 0.08	2.44 ± 0.36	93 ± 26	89 ± 7
30.5	0.25 ± 0.09	5.99 ± 0.61	162 ± 58	138 ± 22	0.14 ± 0.05	3.32 ± 0.34	90 ± 32	76 ± 12
31.5	0.27 ± 0.12	14.39 ± 1.61	81 ± 45	138 ± 11	0.15 ± 0.07	8.05 ± 0.90	45 ± 25	77 ± 6
32.5	0.40 ± 0.16	18.08 ± 1.68	<64	158 ± 12	0.20 ± 0.08	9.15 ± 0.85		80 ± 6
33.5	0.69 ± 0.14	22.86 ± 1.99	<43	138 ± 18	0.42 ± 0.09	14.08 ± 1.23		85 ± 11
34.5	0.36 ± 0.11	14.95 ± 1.58	<89	137 ± 24	0.26 ± 0.08	10.92 ± 1.16		100 ± 18
35.5	0.20 ± 0.06	11.26 ± 0.99	<85	122 ± 13	0.12 ± 0.03	6.49 ± 0.57		71 ± 7
36.5	0.44 ± 0.15	8.66 ± 0.99	<51	76 ± 6	0.22 ± 0.08	4.26 ± 0.49		38 ± 3
37.5	0.23 ± 0.08	6.90 ± 0.59	<50	75 ± 8	0.15 ± 0.05	4.67 ± 0.40		51 ± 5
38.5	0.09 ± 0.03	3.91 ± 0.41	<55	75 ± 9	0.06 ± 0.02	2.51 ± .26		48 ± 5
39.5	<0.04	2.70 ± 0.28	<49	71 ± 7		1.85 ± 0.19		48 ± 5
40.5	<0.04	1.95 ± 0.19	<77	60 ± 2		1.32 ± 0.13		40 ± 1
41.5	<0.06	0.83 ± 0.14	<25	52 ± 5		0.50 ± 0.08		31 ± 3
42.5	<0.04	1.01 ± 0.14	<12	56 ± 4		0.73 ± 0.10		41 ± 3
43.5	<0.09	0.53 ± 0.16	<45	38 ± 6		0.36 ± 0.11		26 ± 4
44.5	<0.05	0.19 ± 0.05	<21	34 ± 5		0.12 ± 0.03		22 ± 3
45.5	<0.04	0.09 ± 0.03	<20	22 ± 3		0.06 ± 0.02		14 ± 2
46.5	<0.06	1.94 ± 0.19	<20	56 ± 5		1.34 ± 0.13		39 ± 4
47.5	<0.05	<0.05		26 ± 3				15 ± 2
48.5	<0.04	0.10 ± 0.05		16 ± 2		0.06 ± 0.03		10 ± 1
49.5	<0.03	0.70 ± 0.13		23 ± 4		0.50 ± 0.09		17 ± 3
50.5	<0.4	0.53 ± 0.15		17 ± 3		0.36 ± 0.10		11 ± 2
51.5	<0.03	0.50 ± 0.15		9 ± 2		0.33 ± 0.10		6 ± 1
52.5	<0.21	0.54 ± 0.13				0.42 ± 0.10		
53.5	<0.3	<0.3						
54.5	<0.2	<0.2						
				Inventory (Bq/m^2)	**1.98 ± 0.63**	**75.94 ± 8.12**	**8970 ± 1300**	**3965 ± 430**

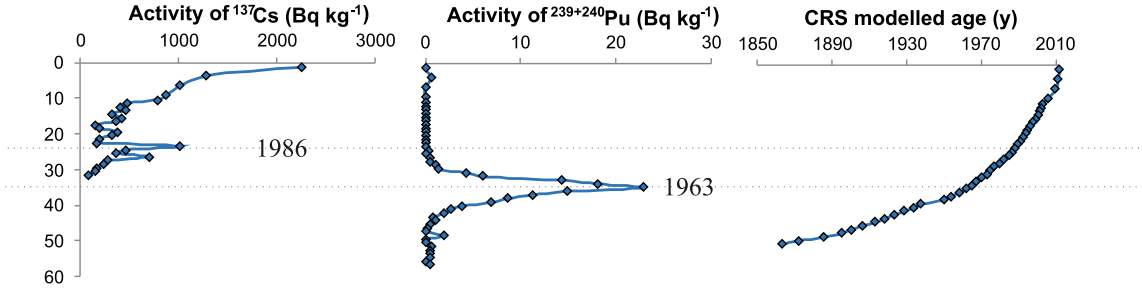

Fig. 2. Comparison of ^{137}Cs and $^{239+240}$Pu activity with CRS model based on ^{210}Pb in Sn1.

Oldfield, 1978). Unsupported activity concentrations of ^{210}Pb, which were determined for each layer by subtracting the supported activities from the total ^{210}Pb activities. The supported level of ^{210}Pb was calculated by using the mean activity of the bottom layers of the peat profile (14 ± 2 Bq kg^{-1}).

The lower section of the profile (52–64 cm) was based on the

Table 2
Radiocarbon dates of Sn1 and Sn2 profiles. Abbreviations: pMC – percent of modern ^{14}C.

Depth [cm]	Material dated	Nr. Lab.	^{14}C date (AMS) [^{14}C BP]	Calibrated date (range 95.4%) [cal. AD]
Sn-1				
35–36	Stems with leaves of *Polytrichum strictum*	Poz-53963	100.66 ± 0.31 pMC	1952–1957 (3.1%) 1990–1996 (91.3%) 2008–2008 (1%)
40–41	Stems with leaves of *P. strictum*	Poz-53964	105 ± 25	1682–1735 (27.5%) 1806–1930 (67.9%)
45–46	Stems with leaves of *P. strictum*	Poz-53965	60 ± 25	1695–1728 (22%) 1812–1854 (20.1%) 1867–1919 (53.3%)
50–51	Stems with leaves of *Calliergon stramineum*	Poz-53966	100 ± 30	1682–1736 (27.1%) 1805–1935 (68.3%)
55–56	Stems with leaves of *C. stramineum*	Poz-53967	170 ± 30	1659–1699 (17.3%) 1721–1818 (50.5%) 1833–1880 (8%) 1916–modern (19.6%)
60–61	Stems with leaves of *C. stramineum*	Poz-53968	200 ± 30	1646–1690 (24.9%) 1729–1810 (51.2%) 1926–modern (19.3%)
63–64	Stems with leaves of *C. stramineum*	Poz-53969	120 ± 25	1680–1764 (31.4%) 1801–1939 (64%)
Sn-2				
11–12	Stems with leaves of *P. strictum*	Poz-66397	106.83 ± 0.35 pMC	1956–1957 (3.1%) 2002–2007 (91.3%) 2008–2008 (1%)
27–28	Stems with leaves of *Sphagnum russowii*	Poz-66399	200 ± 30	1646–1690 (24.9%) 1729–1810 (51.2%) 1926–modern (19.3%)
43–44	Stems with leaves of *S. russowii/lindbergi*	Poz-55190	120 ± 35	1677–1765 (33.4%) 1773–1777 (0.8%) 1800–1940 (61.2%)
52–53	Stems with leaves of *Drepanocladus* sp.	Poz-55191	960 ± 50	990–1186 (95.4%)
63–64	Stems with leaves of *S. russowii*	Poz-56357	1710 ± 35	246–401 (95.4%)

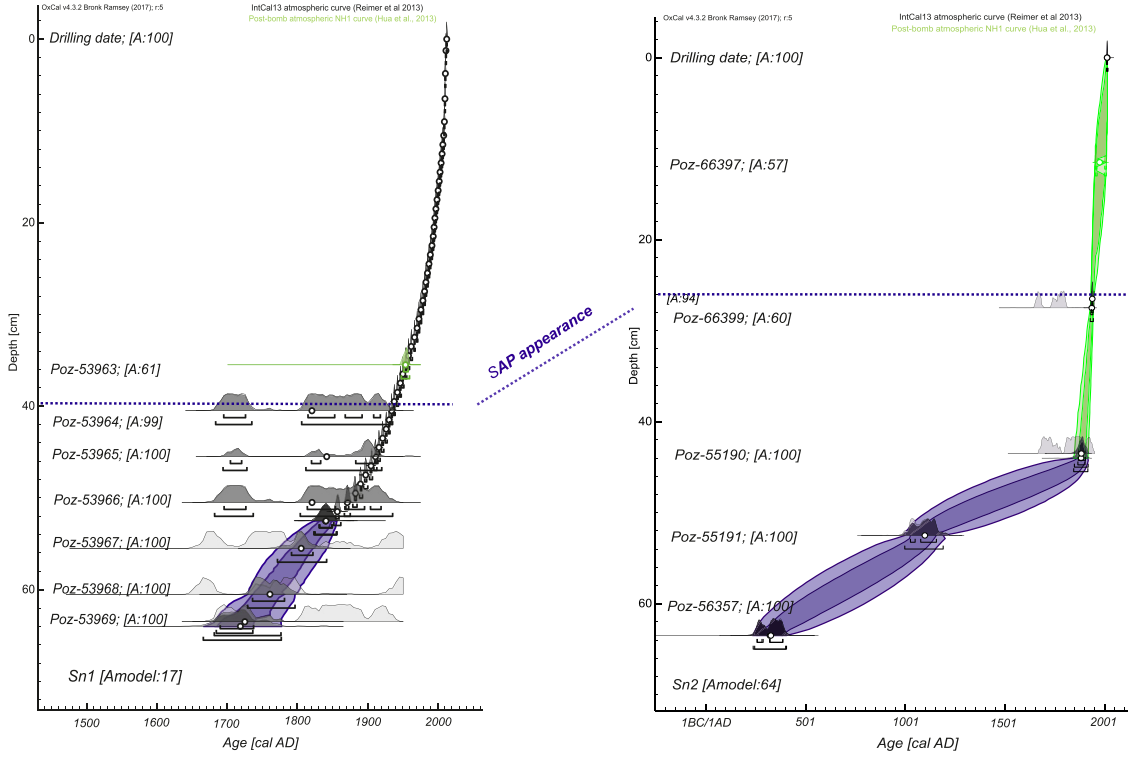

Fig. 3. Age-depth models of both profiles. SAP – spheroidal aluminosilicates.

Bayesian age-depth model constructed using the mixed ^{210}Pb (date from a depth of 52.5 cm introduced using *C_Date* command) and ^{14}C dates. In the case of the Sn2 model, the calendar date AD 1938 ± 2 was introduced (using *C_Date* command) at a depth of

26.5 cm as an extrapolated date of SAP presence in Sn1 (see Fig. 3). Moreover, we used one boundary (*Boundary* command) at a depth of 44 cm due to the rapid change in bulk density (Suppl.2), which might be a trace of two sections of different peat accumulation rates (see Fiałkiewicz-Kozieł et al., 2014, Fiałkiewicz-Kozieł et al., 2015b). For the better readability of the modelled dates, they were expressed as μ values (cal. AD) in the following sections of text.

2.5. Pb, Zn, Cu, Ni, Cr, Sr, Ti, Al, and REE concentrations

Peat samples were dried at 105 °C prior to ashing at 550 °C and acid digestion in Teflon Savillex® beakers. Acid digestion consisted of two steps. First, samples were treated with 4,5 ml of suprapure 65% HNO_3 and 0,5 ml of 45% HF for 48 h at 130 °C. They were then evaporated and treated with 1 ml of concentrated HCl for 24 h in 90 °C. After final evaporation, residues were diluted in 10% HNO_3 and measured using ICP-MS at the UAM for trace metals and at *Observatoire Midi-Pyrénées* (Toulouse, France) for Rare Earth Elements. All measurements were performed in duplicate. NIMT (peat, Yafa et al., 2004) and CTA-OTL-1 (tobacco leaves) certified reference materials were used to monitor the accuracy of measurements. Certified value of NIMT equals: Al - 3692 ± 347 mg kg^{-1}; Cr - 6.36 ± 0.44 mg kg^{-1}; Cu - 5.28 ± 1.04 mg kg^{-1}; Fe - 921 ± 84 mg kg^{-1}; Pb - 174 ± 8 mg kg^{-1}; Ti - 357 ± 18 mg kg^{-1}; Zn - 28.6 ± 1.9 mg kg^{-1}, La −1.24 ± 0.03 mg kg^{-1}, Sm − 0.194 ± 0.005 mg kg^{-1}. Measured CRM values fall within 97% of the certified values for Al, Ti, Cr, Cu, Fe, Pb, Zn, and 85–86% for La and Sm. The analytical deviation is less than 5%.

The accumulation rate (AR) was calculated using concentration ($\mu g\, g^{-1}$) of element, bulk density, and peat accumulation rate using the following equation:

AR (mg m^{-2} yr^{-1}) = concentration* BD (g cm^{-3})*PAR (cm y^{-1}) *10.

The dust flux was calculated using the sum of REE concentrations ($\mu g\, g^{-1}$) in the bulk peat using the following equation (Shotyk et al., 2002):

$$\text{Dust flux}\left(\text{g m}^{-2}\text{yr}^{-1}\right) = \left(\sum [\text{REE}]_{\text{sample}} \Big/ \sum [\text{REE}]_{\text{UCC}}\right)^{*} \text{PAR}\left(\text{cm y}^{-1}\right)^{*} \text{BD}\left(\text{g cm}^{-3}\right)^{*} 10,000$$

were Σ $[REE]_{sample}$ is the sum of REE concentrations ($\mu g\, g^{-1}$) in a sample, Σ $[REE]_{UCC}$ is the sum of REE concentrations in the upper continental crust (144.3 μg g^{-1}; Wedepohl, 1995), PAR is the peat accumulation rate (cm yr^{-1}) calculated according to formula (h2-h1)/(y1-y2), where h-depth, y-age, and BD is the bulk density (g cm^{-3}).

2.6. Pb isotopes

Ten to 500 mg of dry peat and rocks powder was taken in order to obtain 2000 ng of Pb in the final solution. The sample powders were ashed (550 °C, 4 h) prior to digestion in 6 ml HF *suprapur* (Merck) + 1 ml HNO_3 65% *cc. sub.* in Teflon beakers (120 °C, 48 h) in class 1000 clean room (UAM, Poznań). Dried residues were dissolved in HBr 6% *cc. sub.* prior to chromatographic separation. Lead was separated using anionic exchange micro-columns (Weis et al., 2005) and sub-boiled distilled acids. The measurements were conducted on TIMS Finnigan MAT-261 special (UAM). The instrumental drift was controlled by standard bracketing using NBS981 standard data (Galer and Abouchami, 1998). Repeated standard measurements for NBS981 equal: $^{208/204}Pb$ = 36.756 ± 0.013, $^{207/204}Pb$ = 15.484 ± 0.018 and $^{206/204}$ Pb = 16.937 ± 0.010 and are comparable with recommended values: $^{206}Pb/^{204}Pb$ = 16.9406 ± 0.0003; $^{207}Pb/^{204}Pb$ = 15.4957 ± 0.0002, $^{208}Pb/^{204}Pb$ = 36.7184 ± 0.0007 (Taylor et al., 2015).

2.7. Mineralogy

The shape, size, morphology, and chemical composition of dust particles were determined in peat samples using the backscattered electron detector of a scanning electron microscope (SEM) equipped with an energy dispersive system (Philips XL30 ESEM/EDS). The accelerating voltage was 15 kV and 10 mm the working distance. Air-dried peat samples were gently homogenised using a corundum mortar and pestle. A thin layer of each homogenised sample was fixed to a double-sided 9 mm carbon tab, placed on an aluminium stub, and carbon-coated prior to analysis.

Mullite content was determined in Sn1 profile using x-ray diffraction (XRD). For the XRD analysis, peat samples were ashed at 550 °C and treated with 1 M HCl for 15 min to remove the acid-soluble ash fraction (Sapkota, 2006). The residue was dried, ground in an agate mortar, and analyzed using a Panalytical X'Pert PRO - PW 3040/60 X-ray diffractometer. The instrument was equipped with a Ni-filtered Cu Kα source radiation (λ = 1.540598 Å) and an X'Celerator strip detector. Samples were scanned within a 2Θ interval of 2.5–65°, with a step size of 0.01° 2Θ and counting time of 300 s. Identification and quantification of mineral phases was done by means of the X'Pert HighScore Plus Software using the newest ICSD database. The detection limit of the XRD method was 0.5–2%, depending on the sample mineral composition. Analytical precision and accuracy were ±3%.

3. Results

3.1. Chronological control (^{210}Pb, ^{14}C)

The ^{210}Pb activities (Table 1) gradually declined with increasing depth and became constant at depths ranging from 52.5 to 54.5 cm, which was consistent with the equilibrium depth of total ^{210}Pb and supported ^{210}Pb (14 ± 2 Bq kg^{-1}). Fig. 2 shows the CRS age-depth relationships of Sn1 peat profile. The peat section 0 - 49 cm accumulated in 149 years, corresponding to an average accumulation rate of 0.53 ± 0.11 cm yr^{-1}.

The data obtained from ^{14}C activity (Table 2) suggests a hiatus in the Sn2 profile. Therefore, for further interpretation, we opted only to use the top 44 cm, which spans a similar time interval comparing to Sn1.

The A_{model} for the Sn1 model revealed 17%, whereas for the Sn2 it was 64% (Fig. 3). The minimum advised as the critical value for the age-depth model robustness is 60% (Bronk Ramsey, 2008). However, in the case of Sn1, plotting numerous ^{210}Pb dates (as calendar dates), even if excluded from the modelling, caused a decrease in A_{model}. If the Sn1 model is plotted without drawing the section 0–52 cm (with ^{210}Pb dates), A_{model} is much higher, and values of modelled dates for the section 52–64 cm are almost identical to the model including ^{210}Pb dates. The chronology based

on ^{210}Pb calculated for the Sn1 profile fit to the results of ^{14}C dating. The analyzed profiles span a period AD 1725–2012 (Sn1) and AD 1894–2012 (Sn2). The σ errors of the modelled dates calculated during the age-depth modelling based on ^{14}C dates were ca. 8–27 years in Sn1 and 2–35 years in Sn2.

3.2. ^{137}Cs, $^{239+240}Pu$

Activity concentrations and inventories of anthropogenic radionuclides (^{137}Cs, ^{238}Pu, $^{239+240}$Pu) are presented in Table 1 and in Fig. 2. The radionuclide inventory is understood here as the activity concentration of a given radionuclide contained in the profile (Bq kg^{-1}) per unit surface area (kg m^{-2}). The activity concentrations of ^{137}Cs range from 81 ± 45 to 2255 ± 104 Bq kg^{-1}. Most of the total Cs activity concentration is retained in the upper four layers (0–9 cm). Two distinct peaks of ^{137}Cs activity can be found at 23.5 cm (1011 ± 48 Bq kg^{-1}) and 26.5 cm depth (699 ± 58 Bq kg^{-1}), and can be attributed to Chernobyl (1986) and Nuclear weapon test (1963) signal (Table 1, Fig. 2).

Activity concentrations of $^{239+240}$Pu range between 0.06 ± 0.04 Bq kg^{-1} to 22.86 ± 1.99 Bq kg^{-1} (dry weight) with a maximum value at 33.5 cm depth. Activity concentrations for ^{238}Pu in this profile are much lower than for $^{239+240}$Pu. The minimum value is < 0.03 Bq kg^{-1}, the maximum equals 0.69 ± 0.14 Bq kg^{-1} at the same depth as $^{239+240}$Pu (Table 1).

3.3. Discrimination of temporal variations in the deposition of Pb, Zn, Cu, Ni, Cr, Ti, Al, Sc, and REE (concentrations and accumulations)

The ash content varied from 0.5 to 6.1% in Sn1 and between 0.7 and 8.2% in Sn2 (see Suppl. 2). Two maxima with higher ash content are observed (5.5–5.1%; 55.5–53.5 cm; AD 1806–1828) and (6.1%; 30.5 cm; AD 1970) in Sn1. The general shape of ash is similar to Ti and Al concentration pattern. Bulk density (BD), used to calculate accumulation rates, varies from 0.02 to 0.11 g cm^{-3} for Sn1 and 0.03–0.10 g cm^{-3} for Sn2. The last two layers of Sn2 (45.5–44.5 cm; AD 1851–1760) were characterised by a higher density – 0.14–0.17 g cm^{-3} (Suppl.2).

Several shifts in concentration and accumulation of investigated elements can be distinguished.

In Sn1 the layer between 50.5 and 62.5 cm (AD 1739–1872) was characterised by the decreased Pb concentration from 218 mg kg^{-1} at the bottom of the profile to twice lower value of 111 mg kg^{-1} at the depth 58.5 cm (AD 1780), which slightly fluctuated till 50.5 cm (AD 1872). The calculated Pb accumulations are the highest at the bottom (62.5 cm) – 20 mg m^{-2} y^{-1} (Fig. 4). The increase in Al and Ti concentration from 57.5 cm to 50.5 cm; (AD 1789–1872) with maximum at 55.5–53.5 cm (AD 1806–1828) is less visible in accumulation rates (comp. Fig. 4). Other elements displayed only minor fluctuations during that time.

In Sn2 the described period was represented by three samples within a depth interval of 45.5 cm–43.5 cm (AD 1760–1883). This layer was characterised by the highest density and low accumulation rates.

The depth from 50.5 cm to 35.5 cm (AD 1870–1954) in Sn1 was characterised by only small variations in both concentration and accumulation of most elements (Suppl.2, Fig. 4). In Sn2, the depth from 43.5 cm to 20.5 cm (AD 1883–1952) reflected a more complex, but comparable trend to Sn1 (Supl.2, Fig. 4). In both profiles, an anomaly in Cr and Ni is observed within the period. In Sn1, a distinct peak in Cr (33 mg kg^{-1}) and Ni (15 mg kg^{-1}) concentrations is seen at 46.5 cm (AD 1904; Fig. 5). The similar, but broaden peak was also observed in Sn 2 at a depth of 33.5 cm (AD 1912) for Al, Ti, Cr, Ni, and Cu and at 31.5 cm (AD 1922) for Cr and Ni (comp. Suppl.2, Figs. 4, Fig.5). Pb also revealed a small increase in concentration as well as accumulation in both profiles.

The peat layer 22.5 cm–35.5 cm (AD 1954–1988) in Sn1 and 10.5 cm–19.5 cm (AD 1955–1978) in Sn2 was characterised by the most pronounced changes in concentrations and accumulations of all elements.

Sn1 presents a substantial increase of elements at the depth 28.5–30.5 cm (1970–1975 AD): Pb (365 mg kg^{-1}), Al (7740 mg kg^{-1}), Ti (595 mg kg^{-1}), Sc (2.86 mg kg^{-1}), Zn (289 mg kg^{-1}), Cu (26 mg kg^{-1}), Fe (6231 mg kg^{-1}), Cr (18 mg kg^{-1}), Ni (13 mg kg^{-1}) (comp. Suppl. 2.) The corresponding increase in accumulation rates was also observed: Pb AR (77 mg m^{-2} y^{-1}) AlAR (1792 mg m^{-2} y^{-1}), TiAR (164 mg m^{-2} y^{-1}), ScAR (0.63 mg m^{-2} y^{-1}), ZnAR (56 mg m^{-2} y^{-1}), CuAR (4.8 mg m^{-2} y^{-1}), FeAR (1858 mg m^{-2} y^{-1}), CrAR (5.15 mg m^{-2} y^{-1}), NiAR (2.3 mg m^{-2} y^{-1}) (comp. Figs. 4 and 5).

In Sn 2 maximum values had a broaden extend (mostly between 11.5 and 17.5 cm; AD 1960–1974) and Pb reached the maximum

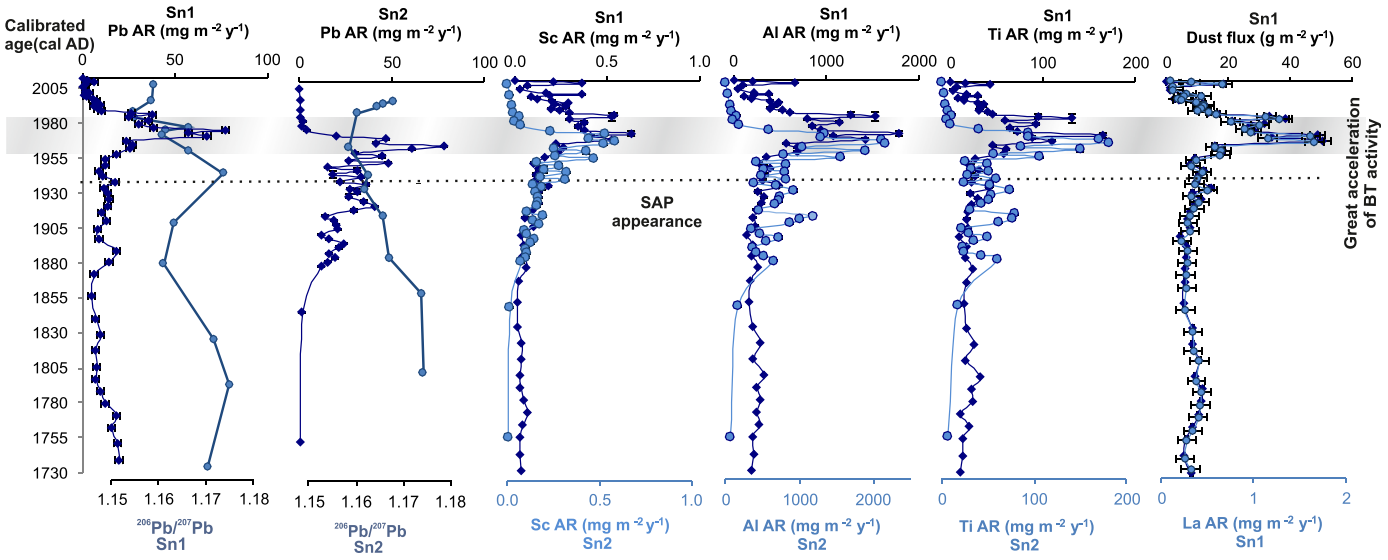

Fig. 4. Geochemistry of Sn profiles vs. depth (Dust flux was based on REE from Sn1).

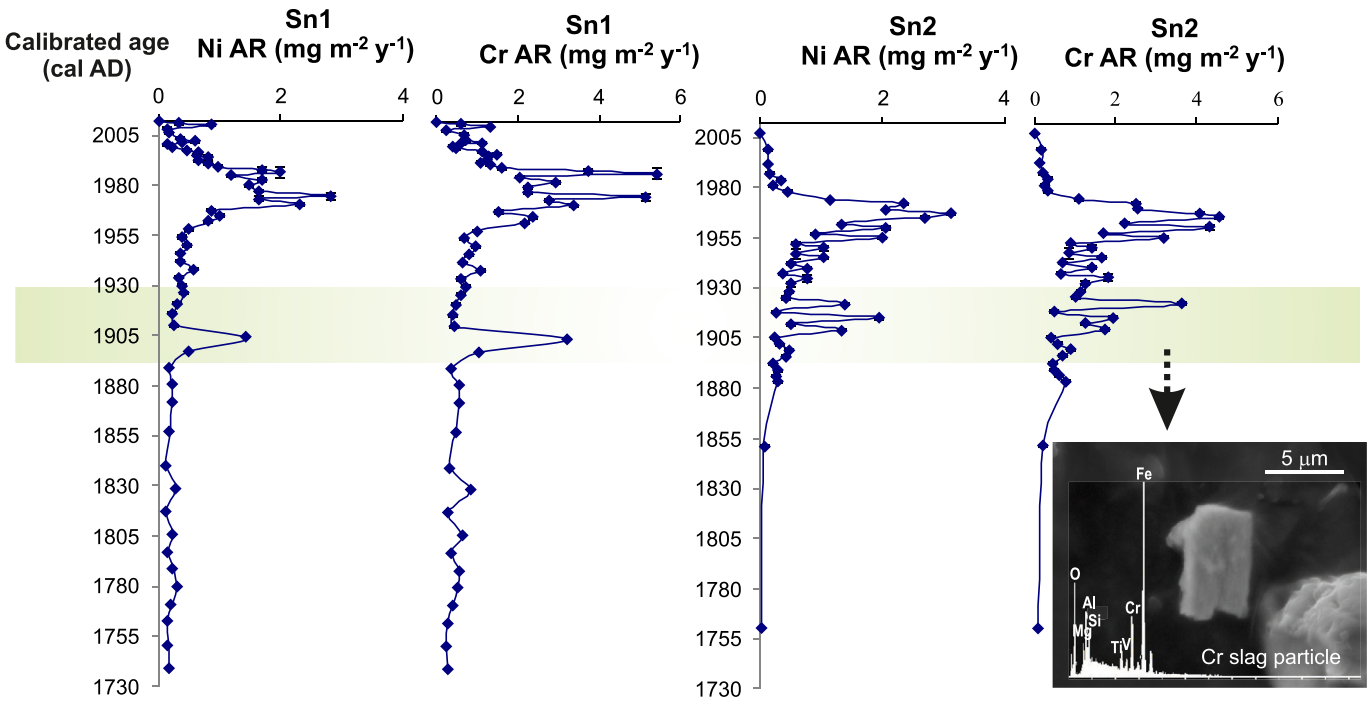

Fig. 5. Concentrations and accumulation rates of Cr and Ni in both profiles confronted with SEM photo slag particle, originated from steel factories.

value (198 mg kg^{-1}) at 14.5 cm (AD 1967) together with Ni (7.9 mg kg^{-1}). Aluminium (5987 mg kg^{-1}), Ti (473 mg kg^{-1}), Cr (13.5 mg kg^{-1}), and Cu (16 mg kg^{-1}) had maximum values of concentration at 17.5 cm depth (AD 1960). Most elements showed then a decreasing trend from 11.5 cm upward except Fe (11,550 mg kg^{-1}) and Zn (109 mg kg^{-1}), which had a maximum at this depth level. The second maximum, visible in Sn1 around AD 1987, was undistinguishable in Sn2, probably due to lesser resolution of the Sn2 age-depth model. The corresponding accumulation rates presented more comparable pattern within the investigated elements and most of them reached the maximum at 14.5 cm (AD 1967): PbAR of (79 mg m^{-2} y^{-1}), ZnAR (38 mg m^{-2} y^{-1}), NiAR (3.1 mg m^{-2} y^{-1}), ScAR (0.58 mg m^{-2} y^{-1}), SrAR (8.3 mg m^{-2} y^{-1}), UAR (0.485 mg m^{-2} y^{-1}). AlAR (2101 mg m^{-2} y^{-1}), TiAR (181 mg m^{-2} y^{-1}), CrAR (4 mg m^{-2} y^{-1}) had the highest AR at 15.5 cm (AD 1965).

Then, from 21.5 cm (AD 1990) and from 10.5 cm (AD1978) in Sn1 and Sn2, respectively, concentrations and accumulations significantly decreased towards the surface, reaching minimum values (Figs. 4 and 5, Suppl. 2).

Rare Earth Element (REE) concentrations assessed for Sn1 are given in the supplementary data (Suppl.2) and presented to show the significance of industrial activity on the cycle of lithogenic elements. The total sum of ∑REE varied from 1.2 to 40 mg kg^{-1} and was used to assess the dust flux (Fig. 4). From the bottom to the 31.5 cm both concentrations and accumulations presented almost straight line with only slight fluctuations. The highest dust accumulation rate was observed at the depth of 30.5 cm (AD 1970) (Fig. 4) and corresponded to other elements in Sn1. The accumulation rate of La as a representative of REE displayed a similar pattern to dust flux reaching maximum values in 1970 (Fig. 4).

3.4. Uranium concentration and isotopes

Slightly elevated values of U concentrations (up to 1 mg kg^{-1}) were recorded in the lower part (31.5–62.5 cm) of Sn1. Three distinct peaks appeared at 30.5 cm (AD 1970; 2.26 mg kg^{-1}), 28.5 cm (AD 1975; 1.54 mg kg^{-1}) and 25.5 cm depth (AD 1982; 1.47 mg kg^{-1}) (Fig. 7). Suppl. 2 presents values of uranium activity for Sn1 which ranged between 1.3 ± 0.2 Bq kg^{-1} to 37.0 ± 3.8 Bq kg^{-1} for ^{234}U, 1.0 ± 0.1 Bq kg^{-1} to 21.0 ± 2.8 Bq kg^{-1} for ^{238}U. The maximum value for ^{234}U and ^{238}U was observed at 24.5 cm depth. Others slightly lower peaks were observed at 29.5 and 48.5 cm depths, respectively. In Sn2 the maximum U concentration (1.06–1.24 mg kg^{-1}) is presented as a broad peak within 11.5–15.5 cm (AD 1965–1974) (Fig. 7).

3.5. Tool for distinguishing sources of deposited elements (Pb isotopes)

Lead isotopic signatures revealed similar age and depth patterns in both peat profiles during the last 100 years. $^{208}Pb/^{204}Pb$ varied from 38.55978 to 38.02255 in Sn1 and from 38.5907 to 37.9157 in Sn2; $^{207}Pb/^{204}Pb$ – from 15.70587 to 15.57680 (Sn1); 15.6728–15.5586 (Sn2); $^{206}Pb/^{204}Pb$ – 18.39197–18.04409 (Sn1) and 18.4274–18.1165 (Sn2) (Table 3; Fig. 4). Generally, the ratio $^{206}Pb/^{207}Pb$ decreased to less radiogenic values from the bottom to the top of the profiles and revealed similarity to the anthropogenic sources (Figs. 4 and 6).

3.6. Mineralogy

The distinguishing of mineral particles in the peat profiles gave an opportunity to further confirm the sources. Spheroidal aluminosilicate fly ash particles (SAP) were the dominant technogenic dust particles detected in the samples using SEM. In the Sn1 profile, SAP were found within a depth range of 0–40 cm and in Sn2 at depths between 0 and 27 cm. This result was used to calculate chronology (comp. 2.4 and Fig. 3). The majority of the SAP particles in the Sn1 profile were within a size range of <1–9.5 µm,

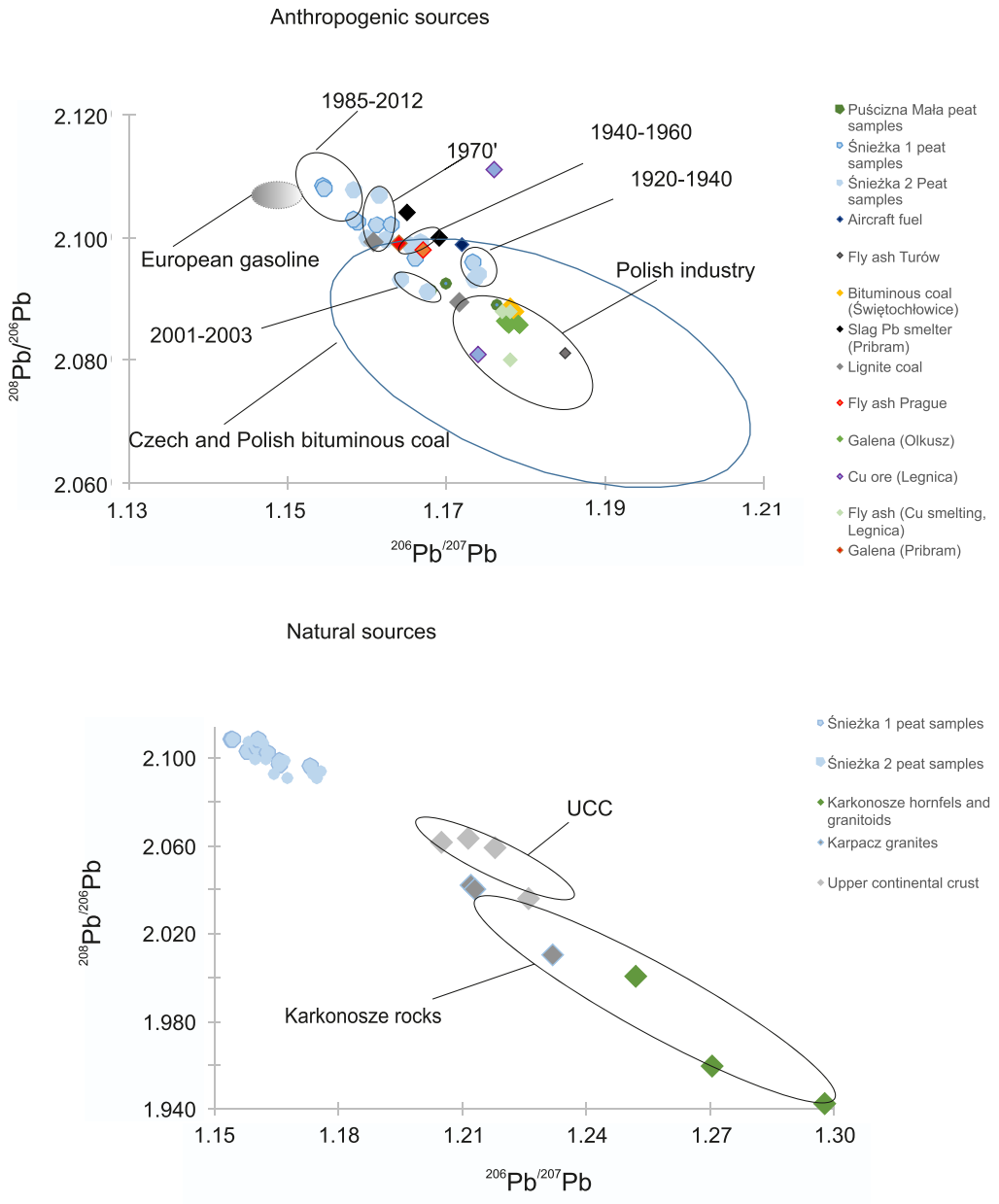

Fig. 6. Sources of Pb in NRS peatland. Values of galena (De Vleeschouwer et al.,2009), bituminous coal in the Czech Republic (Mihaljevič et al., 2009), UCC (Millot et al., 2004; Hemming and McLennan, 2001; Grousset et al., 1994; Asmeron and Jacobsen, 1993), granitoids (Tyszka et al., 2012) and Tab.3, hornfels – Tab.3, fly ash Pribram (Komarek et al., 2008), fly ash Turów- Tab.3, Cu ores, bituminous coal (Tyszka et al., 2012), aircraft fuel – Tab.3; Slag Pb smelter (Ettler et al., 2004).

independent of the depth, which indicates the long-range transport. The mean value was 2.4 and the median - 2.0 μm (n = 180). A small number of much larger (up to 50 μm), less regular, and highly porous aluminosilicates were found within a depth range of 25–35 cm in Sn1.

Mullite is a constant component of the peat ash within a depth range 18–40 cm (AD 1938–1995) and its content is more elevated (9.9–13.3%) between 23 cm and 33 cm depth (AD 1962–1988). It accounts for 1.6–13.3% of the crystalline constituents of the ash. The other crystalline phases detected in the samples in decreasing amounts are as follows: quartz (53.7–91.8%), feldspars (6.8–31.1%), layered aluminosilicates (mainly muscovite and illite <0.5–9.9%), and coesite (up to 5.5%). Hematite (up to 5.8%) is present only in the upper part of the profile.

4. Discussion

Past pollution and environmental changes have been investigated using mountain peatlands for example in Etang de la Gruyère (1005 m a.s.l.) in Switzerland (Shotyk, 1996; Shotyk et al., 1998, 2002), Black Forest (1044 m a.s.l.), Harz Mts (820 m a.s.l.) (Kempter and Frenzel, 2000; Aubert et al., 2006; Gałka et al., 2019) in Germany, Kovářská Bog (870 m a.s.l.; Bohdálková et al., 2018), Bozi Dar (993–1035 m a.s.l.; Veron et al., 2014) Ore Mountains in the Czech Republic, Motianling (about 1700 m a.s.l.) in China (Bao et al., 2010, 2012, 2015), French Pyrenees (1640 m a.s.l. Hansson et al., 2017). Some of these peatlands are located on medium altitudes and have received dust mostly from vertical transport because of orographic

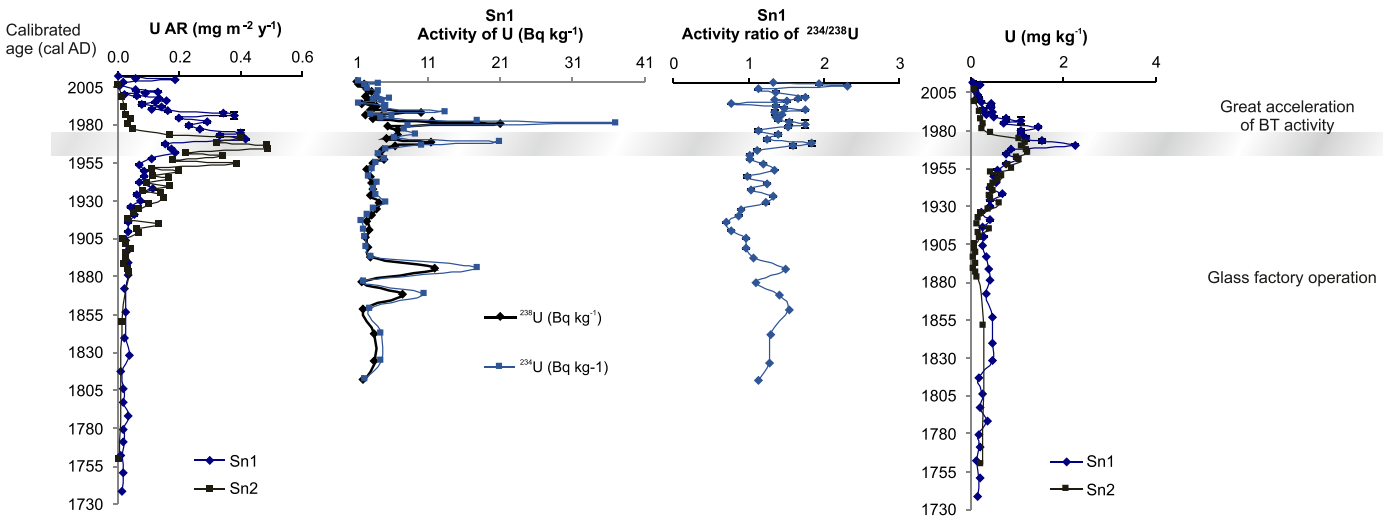

Fig. 7. Concentrations and accumulation rates of uranium in Sn1 and Sn2 as well as activity of ^{234}U, ^{238}U and $^{234}U/^{238}U$ ratio in Sn1.

Table 3
Pb isotopic signature of peat samples, Karkonosze rocks, aircraft fuel, lignite from mine Turów and fly ash from power plant Turów.

Sample	$^{208}Pb/^{204}Pb$	2σ	$^{207}Pb/^{204}$ Pb	2σ	$^{206}Pb/^{204}$ Pb	2σ	$^{208}Pb/^{206}$ Pb	2σ	$^{206}Pb/^{207}$ Pb	Age (cal AD)
Sn1 10	38.03005	0.0054	15.62032	0.0019	18.10171	0.002	2.102277	0.000094	1.158857	2008
Sn1 18	38.02255	0.0069	15.62062	0.0018	18.09471	0.0029	2.102677	0.000074	1.158387	1997
Sn1 23	38.18731	0.0037	15.68999	0.0016	18.11321	0.0016	2.10821	0.00001	1.154443	1989
Sn1 25	38.03518	0.008	15.62656	0.0062	18.04409	0.0076	2.107892	0.000144	1.154706	1985
Sn1 28	38.18539	0.011	15.603	0.0042	18.19608	0.0056	2.098303	0.00016	1.166191	1978
Sn1 29	38.0967	0.0054	15.60748	0.0047	18.12604	0.0056	2.101796	0.000064	1.161369	1976
Sn1 30	38.13942	0.005	15.64146	0.002	18.15352	0.0023	2.104438	0.000056	1.160602	1973
Sn1 33	38.08321	0.0062	15.5768	0.0024	18.16475	0.0029	2.096501	0.000064	1.166141	1962
Sn1 37	38.44224	0.0047	15.6313	0.0019	18.34241	0.0023	2.095801	0.000084	1.173441	1946
Sn1 45	38.33044	0.0034	15.67904	0.001	18.23704	0.00095	2.101797	0.00009	1.163147	1911
Sn1 49	38.34988	0.0034	15.6684	0.0013	18.18967	0.0014	2.108312	0.00004	1.160915	1882
Sn1 53	38.5393	0.0022	15.69733	0.00073	18.38912	0.00069	2.095686	0.000053	1.171481	1829
Sn1 56	38.52527	0.0056	15.65633	0.0064	18.39197	0.007	2.0947	0.000071	1.174731	1797
Sn1 62	38.55978	0.0073	15.70587	0.0026	18.3789	0.0028	2.097991	0.000145	1.170194	1739
Sn2 7	38.05277	0.0021	15.58308	0.00083	18.19791	0.00083	2.090989	0.000046	1.167799	2003.2
Sn2 8	38.22255	0.0024	15.6253	0.0008	18.21482	0.0008	2.098391	0.000076	1.165726	2002.1
Sn2 9	37.91569	0.0033	15.55858	0.0012	18.11649	0.0014	2.092889	0.000066	1.164406	2001
Sn2 11	37.96922	0.0031	15.58799	0.0011	18.08258	0.001	2.099691	0.000064	1.160033	1998.3
Sn2 13	38.24189	0.0035	15.66424	0.0015	18.1456	0.0017	2.10751	0.000042	1.158409	1984.8
Sn2 15	38.05584	0.0025	15.59224	0.0009	18.12474	0.0011	2.099525	0.00007	1.16242	1973.3
Sn2 17	38.38368	0.0032	15.68434	0.0012	18.2203	0.0014	2.10661	0.000053	1.161687	1967.7
Sn2 21	38.21799	0.0031	15.62475	0.001	18.2114	0.001	2.09851	0.000074	1.165549	1956.7
Sn2 27	38.29989	0.0039	15.63554	0.0016	18.2448	0.0018	2.09911	0.000037	1.16688	1940
Sn2 32	38.37868	0.0035	15.62355	0.0013	18.33689	0.0015	2.09291	0.000056	1.17367	1925.7
Sn2 43	38.44178	0.0037	15.63644	0.0014	18.35909	0.0015	2.09391	0.000072	1.174122	1894
Sn2 49	38.3288	0.0019	15.60277	0.00062	18.33207	0.00059	2.090741	0.000054	1.174924	1385
Sn2 53	38.38283	0.0024	15.62275	0.00086	18.35595	0.0011	2.091011	0.000036	1.17495	1027
Karkonosze granite	39.01072	0.00496	15.66553	0.00190	19.61299	0.00230	2.00071	0.00004	1.2520	–
Karkonosze granite	39.34268	0.01410	15.69888	0.00560	20.37302	0.00760	1.94245	0.00006	1.2977	–
Hornfels (Śnieżka)	38.65343	0.01990	15.61900	0.00770	19.84126	0.01010	1.95959	0.00014	1.2703	–
Aircraft fuel	38.56078	0.00390	15.67752	0.00120	18.37255	0.00130	2.09876	0.00007	1.1719	–
Lignite – Turów mine	38.50803	0.00480	15.61832	0.00190	19.30891	0.00230	1.99423	0.00006	1.2363	–
Lignite – Turów mine	38.07841	0.00370	15.55436	0.00130	18.22324	0.00150	2.08951	0.00005	1.1716	–
Lignite – Turów mine	37.88724	0.00290	15.54743	0.00150	18.04762	0.00230	2.09923	0.00007	1.1608	–
Fly ash Turów power plant	38.69995	0.00190	15.69176	0.00110	18.59536	0.00084	2.08105	0.00007	1.1850	–

barrier of higher summits, which block more lateral transport of particles. The obtained data reveal that Śnieżka shows a more lateral pattern of dust distribution due to the fact of being the highest summit in this part of Europe (see Fig. 1). The detected signals are defined to be more regional due to the fact of being recognized in other countries (comp. discussion below).

4.1. Steel factories signal

An increase in Cr and Ni accumulation was described in peatlands from the United States (Cole et al., 1990), Poland (De Vleeschouwer et al., 2009), Belgium (Allan et al., 2013), the Czech Republic (Bohdálková et al., 2018) and Germany (Gałka et al., 2019). A distinguishable signal around 1904 ± 15 in Sn1 and from

1922 ± 7–1928 (±6) in Sn2 in the Cr–Ni accumulation profiles is also observed in Śnieżka, with only slight fluctuations in trace and REE accumulation rates (Fig. 5). Ni and Cr are suggested to be immobile in peat bogs (Krachler et al., 2003; Allan et al., 2013), but research indicating mobility also occurred (Nieminen et al., 2002; Ukonmaanaho et al., 2004). Despite the existence of these contradicting conclusions, the repeatable signal in both profiles (Sn1, Sn2) gives us confidence in the possible immobility of those elements. A sharp increase in Cr and Ni in Cowles bog (USA, Northern Indiana), observed in 1928–1942, was explained as booming stainless-steel industry (Cole et al., 1990). The invention of stainless steel in 1912 was a milestone and caused the boosting of industrial development in many countries (Corker, 2016). In Europe, the leading producer of Cr–Ni steel was Krupp company, the owner of many steel factories, located in Germany (Ruhr area, Kiel) and Poland (presently), for example in Szklary (Ger. Glasendorf) (see Fig. 1). The Szklary Ni-Steel factory was located about 120 km east of Śnieżka, and operated from 1901 to 1920 on both local and imported Ni ores (Furmankiewicz and Krzyżanowski, 2008). In Belgium, the Cr–Ni increase was attributed to industrial activities from the Ruhr region, also belonging to the Krupp company, 300 km from the investigated peatland (Allan et al., 2013). The Ruhr stainless steel industries and their use of Ni–Cr steel alloys promoted the emission of these two metals (Corker, 2016). In the Słowińskie Błota bog (Northern Poland), 7 mg kg^{-1} was detected in peat layer accumulated in AD 1920, similarly to the NRS bog, but the accumulation rate in Słowińskie Błota was much lower (De Vleeschouwer et al., 2009). The Słowińskie Błota bog is located about 400 km to Kiel and could also be affected by nearby Krupp steel factories. While the exact number of steel factories operating during that time is unknown, the use of primitive technology without particulate-emission control systems has certainly contributed to the elevated Ni and Cr accumulations found in the NRS peat profiles. This is also supported by slag particles found in the Sn1 peat profile at the depth of the highest Cr–Ni concentration and accumulation (Fig. 5). Such particles were not found in the topmost layers. The elevated peak in Cr and Ni in the 1970s and 1980s, together with other investigated elements, is attributed to extensive brown coal combustion (comp. Figs. 4 and 5).

4.2. Uranium processing signal

The Sudetes lie in the northern part of the Bohemian Massif, the most important uranium ore district in Europe with many deposits of various sizes, both in the Czech Republic and bordering eastern Germany. The total historical uranium production is estimated at 350 Mt for the region (OECD-IAEA, 2003). The total production of uranium ores in Germany (Wismut company) from 1946 to 2012 was c. 220 Mt. In Czechoslovakia (presently as the Czech Republic and Slovakia), the total uranium production from 1945 to 2017 was c. 112 Mt (Diehl, 2011). Before becoming a strategic material, uranium was also mined as a by-product during the exploitation of copper, iron, or arsenic ores and used for colouration in glass and porcelain industries (Procházka et al., 2009). Natural uranium consists of three alpha radioactive isotopes: 99.2745% of ^{238}U, 0.7200% of ^{235}U, and 0.0054% of ^{234}U (Boryło and Skwarzec, 2014). The specific activity of ^{238}U is much lower (1.24 × 104 Bq g^{-1}) compared to ^{234}U (2.30 × 108 Bq g^{-1}) (Browne and Firestone, 1986). A$^{234}U/^{238}U$ ratio close to 1 is typically found in natural samples including rock samples and sediments (Boryło, 2013). The moss *Pleurozium schreberi* from northern Poland revealed the isotopic ratio also around 1 (Boryło et al., 2017).

A recognizable regional signature is seen in the U record of Śnieżka peat profiles (Fig. 7). In Sn1 and Sn2 profiles, two periods in uranium deposition can be distinguished. The obtained values are two orders of magnitude higher than values reported in the mountainous Etang de la Gruère bog in Switzerland (Krachler and Shotyk, 2004). Moreover, a strong disequilibrium in a$^{234}U/^{238}U$ ratio is observed. From 1872 to 1897, two distinct peaks with value 1.49–1.53 are observed. From 1973 several distinct shifts are observed with value 1.59–1.79, reaching the maximum of 2.3 in 2009. The main natural source of uranium in the air is rock weathering (Boryło and Skwarzec, 2014). The geochemical explanation of radioactivity imbalance is the looser bonds of ^{234}U atoms in mineral structures, making them easier to leach during physicochemical erosion (Fleischer and Raabe, 1978). Industrial activities, fossil fuel combustion, phosphate fertilizers in agriculture, and domestic and industrial sewage trigger the increase of uranium concentration and disequilibrium of $^{234}U/^{238}U$ ratio (Boryło, 2013; Boryło and Skwarzec, 2014).

The elevated values, together with an increased ^{234}U activity coincide with the discovery of uranium and increasing mining and processing of uranium as well as coal combustion. The U peak around 1840–1890 is interpreted here as originating from the glass/porcelain industry. The glassworks used local rock material and charcoal, both enriched in uranium, as well as pure uranium for colouration. This glass industry gained its highest popularity around 1880–1920 (Rene, 2008). Several glassworks existed in the Sudetes and in the South of Bohemia as well as in Germany, Austria, England, and France during that time (Rene, 2008; Procházka et al., 2009).

The increase in uranium accumulation rate starting from the year 1938 and reaching a maximum in the 1970s–1980s, reflects the pollution from fossil fuels' burning, in line with other proxies. Uranium was classified as a coalphile element by Ketris and Yudovich (2009). The brown coals from the nearby Turów coal field have twice higher U content (4.4 mg kg^{-1}) than the average for Polish brown (2.2 mg kg^{-1}) and hard (2.0 mg kg^{-1}) coals (Bojakowska et al., 2008). The uranium concentration of Czech brown coal varies from 0.60 to 4.03 mg kg^{-1} (Bouska and Pesek, 1999). The mining of uranium ores constitutes an additional source of uranium supply to the atmosphere. Taking into account the fact that industrial activities promote the release of ^{234}U to the environment, we propose here that ombrotrophic peatlands can record the influence of humans on the biogeochemical cycle of uranium.

4.3. Chernobyl signal

The Chernobyl accident caused a dramatic release of many radionuclides, which were dispersed through Europe. The highest content of radionuclides reached the Belarus boundary, then split up towards Scandinavia and the southwestern part of Europe. It appeared in Poland two days after the accident. The most polluted area was the Opolskie (Southern Poland) and the part of Lower Silesian voivodeship, including Karpacz town, located at the feet of Śnieżka (Łukaszek –Chmielewska et al., 2018). The heterogeneous pattern of radionuclide fallout was caused by diverse weather conditions.

There is a strong increase of ^{137}Cs in the upper 4 cm of Sn1, probably due to plant retention (See Fig. 2 and Table 1). Similarly to K, ^{137}Cs can be uptaken by roots (Gerdol et al., 1994) and accumulated in living plants. This phenomenon was also described elsewhere in peatlands (Mróz et al., 2017; Fiałkiewicz-Kozieł et al., 2014; Rosen et al., 2009). We suspect that the ^{137}Cs from Chernobyl may be present in the top peat layers. The total inventory of ^{137}Cs in Sn1 is 8970 ± 1300 Bq m^{-2} (Table 1). The estimated weapons Cs deposition for Poland is 982 Bq m^{-2}, but the mean total

(including Chernobyl) value for ^{137}Cs inventory for Poland is 3770 Bq m^{-2} (Stach, 1996). In the Upper Odra valley (SW Poland), the ^{137}Cs inventory equaled to 5230 Bq m^{-2} (Poręba and Bluszcz, 2007). The mean inventory value for the other regions of southern Poland (e.g. Opole and Katowice provinces) equals to 11,240 Bq m^{-2} and 6800 Bq m^{-2} respectively (Stach, 1996), but the contribution of ^{137}Cs of Chernobyl fallout in this region is about 80% of the total ^{137}Cs fallout. The mean value for ^{137}Cs inventory for the Tatra National Park (Mietelski et al., 2008) in southern Poland is 7800 Bq m^{-2}, and this value is comparable with Sn1. In the Czech Republic, the area from Śnieżka toward Prague was characterised by 3000–10,000 Bq m^{-2}, but on NW from Śnieżka only 1000–3000 Bq m^{-2} was detected (Hanslík et al., 2018). The results are in good agreement with previous studies, conducted in higher elevation mountains such as the Tatra Mts.

4.4. Nuclear weapon test signal

There are two main sources of plutonium isotopes: global radioactive atmospheric fallout due to nuclear weapon tests and the Chernobyl accident. Plutonium from the global fallout was spread worldwide, but Pu from the Chernobyl accident was only dispersed in the form of fuel particles and was deposited mostly in the north-eastern and eastern parts of Poland (Mietelski et al., 2016). Non-volatile elements like Pu can be transported on larger aerosol "hot particles" (Cuddihy et al., 1989; Devell et al., 1986). The average deposition of global fallout of $^{239+240}$Pu for Poland was 58 Bq m^{-2} (UNSCEAR, 1982), and about 4% of the activity of $^{239+240}$Pu is due to the average ^{238}Pu deposition from weapon tests and fallout after the SNAP-9A satellite accidental burn up over the Madagascar. Therefore, we observed lower values for ^{238}Pu than for $^{239+240}$Pu.

The observed maximum of $^{239+240}$Pu activity concentrations characterize the global fallout peak of 1963 and is commonly used to identify specific horizons in lake sediments, peat, and other deposits, as well as to estimate their accretion rates. The total inventory of $^{239+240}$Pu and ^{238}Pu is 76.6 ± 7.8 Bq m^{-2} and 2.20 ± 0.71 Bq m^{-2}, respectively. The value of $^{239+240}$Pu deposition is slightly higher to the Polish average of 58 Bq m^{-2} predicted by the UNSCEAR (1982). It is, however, in line with values found by Mietelski et al. (2008) in the Kościeliska Valley area, Tatra Mts. The ^{238}Pu/$^{239+240}$Pu activity ratios were calculated for layers with the maximum activity of these isotopes. In the Sn1, the values: 0.018 ± 0.005 to 0.051 ± 0.019 with a mean value of 0.029 ± 0.010 correspond to global fallout, including the SNAP-9A satellite crash (0.03–0.05) and there is no presence of Chernobyl-origin plutonium. The ^{238}Pu/$^{239+240}$Pu activity ratio for Chernobyl fallout is ~0.50 (Mietelski and Wąs, 1995) detected only in northern Poland (Mietelski et al., 2016). In the Czech Republic the deposition of plutonium isotopes over former Czechoslovakia (Hölgye and Filgas, 1995) varies from 10.2 to 108.8 Bq m^{-2} for $^{239+240}$Pu and from <0.5 to 6.2 Bq m^{-2} for cumulative ^{238}Pu (Hölgye and Filgas, 1995; Hölgye and Malý, 2000).

4.5. Coal combustion central Europe signal

In Europe, lead in the atmosphere originated from ore processing, coal combustion, and gasoline usage (Pacyna et al., 2007). The isotopic signature of galena and coal in Central European records are very similar in areas where coal is the main source of lead (Vile et al., 2000; Novak et al., 2003; Cimova et al., 2016). Leaded gasoline, which was an important source of lead in western European countries, is hidden here by coal signatures (Fig. 6). The ^{206}Pb/^{207}Pb signature of aircraft fuel (1.172) taken presently from the main producer of fuel (Laboratory Warter fuels, Płock, Poland) (Table 3), similar to Polish leaded gasoline used in the 1980s (1.174, Yao et al., 2015), is placed within the range of coal signature.

SAP and mullite which form during industrial coal combustion have been deposited on the Śnieżka plateau since 1938 (Figs. 3 and 4), which is later than the electrification of Black Triangle (Krajniak, 2017) and later than the occurrence of fly ash particles in peatlands located close/within coal-based regions (Yang et al., 2001; Smieja-Król et al., 2019). Lower abundance and technological restrictions (e.g., lower chimneys resulting in proximal dissemination only) of the earlier times of industrialisation (before ~1950) often give a local/regional signal (Waters et al., 2018) registered in the Śnieżka Mountain only by the occurrence of larger (up to 50 μm) porous aluminosilicates at the depth of 25–35 cm (1912–1942). Such particles were also found in Puścizna Mała (Fiałkiewicz-Kozieł et al., 2011; Smieja-Król and Fiałkiewicz-Kozieł, 2014) as well as in Bagno Mikołeska in the Silesian Upland, southern Poland (Smieja-Król and Fiałkiewicz-Kozieł, 2014) and unfound in Mukhrino peatland located in western Siberia (Fiałkiewicz-Kozieł et al., 2016), far from human activity. We hypothesise that they came from closely located emitters via local transport, and because they occurred only before 1950, the main cause was the primitive technology of heating, e.g. from tourist infrastructure at Śnieżka (comp. Kicińska, 2019). However, further studies should be undertaken to support this hypothesis.

The acceleration of coal usage is seen in all proxies shortly after 1970 when the total production of lignite was 260 Gt in Germany (Öko-Institut, 2017), 80 Gt in Czech Republic (Vrablik et al., 2017) and 39 Gt in Poland (Kasztelewicz, 2018). The 1970s are characterised by the highest Pb accumulation rate in both profiles: Sn1 (77 mg m^{-2} yr^{-1}) and Sn2 (78 mg m^{-2} yr^{-1}) (Fig. 4) comparable to other peatlands from the Black Triangle region (60–65 mg m^{-2} yr^{-1}; Novak et al., 2008) or other heavy-industry impacted regions (100 mg m^{-2} yr^{-1}; Allan et al., 2013). The highest sum of REE and other elements regarded as lithogenic was also noted for that time and attributed to lignite combustion (comp. with dust flux in Fig. 4., which is calculated based on ∑REE and La AR as REE representative). It is known that coals contain REE, Th, U, Ti, Zr, and Sc (Bouska and Pesek, 1999; Ketris and Yudovich, 2009; Dolnickova et al., 2012), and that these elements are further concentrated in fly ash (e.g., Vassilev et al., 2001; Jones et al., 2012) emitted in significant amounts during coal combustion. The peak of the booming industry in the 1970s is also recorded by less radiogenic ^{206}Pb/^{207}Pb ratios (1.161–1.162), distinguished in both profiles (Figs. 4 and 6, Table 3). This is comparable to isotopic signature of the Czech industry (Novak et al., 2003, 2008; Zuna et al., 2011; Bohdálková et al., 2014) and soils in Colditz (eastern Germany within the Black Triangle) (1.161–1.167) (Haack et al., 2003). The isotopic signature of Colditz soil (see Fig. 1) was significantly distinct from the Pb isotopic signature of other locations in western or southern Germany.

The Pb signature is also distinct from the rest of the Polish industry (Cu exploitation, Turów power plant activity) located in the Lower Silesian area (comp. Fig. 6, Table 3, Tyszka et al., 2012).

Despite its location in the Black Triangle, the Śnieżka peatland reveals similarities in its Pb isotopic composition with north Poland (De Vleeschouwer et al., 2009), the Czech Republic (Novak et al., 2003), Switzerland (Weiss et al., 1999) and Belgium (De Vleeschouwer et al., 2012). It, however, displays discrepancies with Puścizna Mała - SE Poland (Fiałkiewicz-Kozieł et al., 2018), where distribution patterns are more local due to their foothill character (comp. Fig. 1). The Tatra mountains act here as an effective barrier for long-range transported pollutants. The closeness of the eastern border with various precipitation regimes and wind

directions, as well the burning of peat and coal influenced significantly the isotopic ratio of Pb in peatlands from SE Poland, while the Śnieżka peatland displays less radiogenic profiles, suggesting that they receive more long-range transported pollutants, mainly from the west because of the dominant westerlies (comp. Figs. 1 and 6).

A second peak is visible around 1982–1986 and can also be attributed to lignite burning. This period is characterised by the highest production of coal in Poland but also by the highest dust emissions in Saxony (Zimmermann and Bothmer, 2000).

From 1987 onwards, a substantial decrease in all element concentration is observed as a result of reinforced pollution management in Europe. The least radiogenic $^{206}Pb/^{207}Pb$ isotopic ratio 1.150 (Figs. 4 and 6, Table 3) is comparable to the values of fly ash originating from waste incinerators (1.14–1.16) from different parts of Europe (Komarek et al., 2008) as well as of unleaded gasoline (1.157) (Haack et al., 2002) and modern aerosols (Bollhöfer and Rosman, 2001), as observed elsewhere in Polish peatlands (De Vleeschouwer et al., 2009).

5. Conclusions

Both peat profiles, sampled in the ombrotrophic mountain peatland, record relatively similar geochemical changes linked to historical industrial activities, despite their different peat accumulation rates. The use of a wide spectrum of geochemical proxies allows distinguishing several broadly recognized sources of pollutants.

1. The Black Triangle industrial activities (the Czech Republic, Germany and Poland) as well as the broad Central Europe coal use caused the most significant changes in the geochemistry of Śnieżka peatland and were the dominant source of pollution and atmospheric emission of most elements such as PHTE (Pb, Zn, Cu, Ni, Cr). All the elements classified as “lithogenic” on a geological viewpoint (Ti, Al, Sc, REE), also increased during 1970’as a result of the intensive use of coal, pointing out that one should be cautious when using them as reference elements to calculate enrichment factors, as part of these lithogenic elements though are issued from anthropogenic activities.
2. The leaded gasoline signal is hidden by the coal isotopic ratio, which has been abundantly used in central Europe. While the local signal linked to Polish industry is weakened by the elevated altitude, long-range transport is distinguishable, despite the severe pollution of the region. It is confirmed by the size of SAP, which varies from <1–9.5 μm and indicates distal particles.
3. Lead isotopes have indicated a significant contribution of the neighbouring industry to the contamination of Śnieżka.
4. Cr and Ni depositions are strongly influenced by Ni ore smelting and production of stainless steel, also attesting of long-range transport, probably from Germany.
5. The $^{239+240}Pu$ activity concentrations fingerprint the global fallout peak of nuclear weapon tests, while Chernobyl signal is confirmed only by ^{137}Cs activity.
6. The uranium activity concentration profile displays a complex pattern, and the section corresponding to AD 1828–1938 is clearly dissociated from the topmost part of the profile. The observed disequilibrium in the $^{234}U/^{238}U$ ratio, exceeding 1.0, indicates an anthropogenic influence on the release of more mobile ^{234}U.
7. Overall, the Sudetes behave like a typical mountain critical zone despite the localisation on lower altitude, and therefore receive more regional, long-range sources of aerosols.

Acknowledgements

This research was funded by the Polish National Centre of Science (NCN) 2011/01/D/ST10/02579 granted to BFK. Jolanta Dopieralska (Isotopic Laboratory, UAM) is thanked for Pb isotopes measurements. We would like to thank Danuta Smółka-Danielowska for providing fly ash and Monika Fabiańska for lignite samples. Barbara Raniś is thanked for technical help with ash content and bulk density. Marie-Josée Tavella and Aurélie Lanzanova are thanked for their help in the preparation and measurement of REE at the Service ICP-MS Observatoire Midi Pyrénées (Toulouse, France). Chuxian Li is thanked for her substantive support.

Appendix A. Supplementary data

Supplementary data to this article can be found online at https://doi.org/10.1016/j.quascirev.2020.106162.

References

Allan, M., Le Roux, G., De Vleeschouwer, F., Bindler, R., Blaauw, M., Piotrowska, N., Sikorski, J., Fagel, N., 2013. High-resolution reconstruction of atmospheric deposition of trace metals and metalloids since AD 1400 recorded by ombrotrophic peat cores in Hautes-Fagnes, Belgium. Environ. Pollut. 178, 381–394.
Appleby, P.G., Oldfield, F., 1978. The calculation of 210Pb dates assuming a constant rate of supply of unsupported 210Pb to the sediment. Catena 5, 1–8.
Arellano, L., Fernandez, P., Tatosova, J., Stuchlik, E., Grimalt, J.O., 2011. Long-range transported atmospheric pollutants in snowpacks accumulated at different altitudes in the Tatra mountains (Slovakia). Environ. Sci. Technol. 45, 9268–9275.
Asmeron, Y., Jacobsen, S.B., 1993. The Pb isotopic evolution of the Earth: inferences from river water suspended loads. Earth Planet. Sci. Lett. 115, 245–256.
Aubert, D., Le Roux, G., Krachler, M., Cheburkin, A., Kober, B., Shotyk, W., Stille, P., 2006. Origin and fluxes of atmospheric REE entering an ombrotrophic peat bog in Black Forest (SW Germany): evidence from snow lichens and mosses. Geochem. Cosmochim. Acta 70 (11), 2815–2826.
Bao, K., Xia, W., Lu, X., Wang, G., 2010. Recent atmospheric lead deposition recorded in an ombrotrophic peat bog of Great Hinggan Mountains, Northeast China, from ^{210}Pb and ^{137}Cs dating. J. Environ. Radioact. 101, 773–779.
Bao, K., Xing, W., Yu, X., Zhao, H., McLaughlin, N., Lu, X., Wang, G., 2012. Recent atmospheric dust deposition in an ombrotrophic peat bog in Great Hinggan Mountain, Northeast China. Sci. Total Environ. 431, 33–45.
Bao, K., Shen, J., Wang, G., Le Roux, G., 2015. Atmospheric deposition history of trace metals and metalloids for the last 200 years recorded by three peat cores in Great Hinggan Mountain, Northeast China. Atmosphere 6 (3), 380–409.
Bergin, M.S., West, J.J., Keating, T.J., Russell, A.G., 2005. Regional atmospheric pollution and transboundary air quality managements. Annu. Rev. Environ. Resour. 30, 1–37.
Bohdálková, L., Novak, M., Stepanova, M., Fottova, D., Chrastny, V., Mikova, J., Kubena, A.A., 2014. The fate of atmospherically derived Pb in central european catchments: insights from spatial and temporal pollution gradients and Pb isotope ratios. Environ. Sci. Technol. 48 (8), 4336–4343.
Bohdálková, L., Bohdálek, P., Břízová, E., Pacherová, P., Kuběna, A.A., 2018. Atmospheric metal pollution records in the Kovářská Bog (Czech Republic) as an indicator of anthropogenic activities over the last three millennia. Sci. Total Environ. 633, 857–874.
Bojakowska, I., Lech, D., Wołkowicz, S., 2008. Uranium and thorium in hard and brown coals from Polish deposits. Gospodarka Surowcami Mineralnymi 24 (2/2), 53–65.
Bollhöfer, A., Rosman, K.J.R., 2001. Isotopic source signatures for atmospheric lead: the Northern Hemisphere. Geochem. Cosmochim. Acta 65, 1727–1740.
Boryło, A., 2013. Determination of uranium isotopes in environmental samples. J. Radioanal. Nucl. Chem. 295 (1), 621–631.
Boryło, A., Skwarzec, B., 2014. Activity disequilibrium between ^{234}U and ^{238}U isotopes in natural environment. J. Radioanal. Nucl. Chem. 300 (2), 719–727.
Boryło, A., Romańczyk, G., Skwarzec, B., 2017. Lichens and mosses as polonium and uranium biomonitors on Sobieszewo Island. J. Radioanal. Nucl. Chem. 311 (1), 859–869.
Bouska, V., Pesek, J., 1999. Quality parameters of lignite of the north bohemian basin in the Czech republic in comparison with the world average lignite. Int. J. Coal Geol. 40 (2–3), 211–235.
Bronk Ramsey, C., 1995. Radiocarbon calibration and analysis of stratigraphy: the OxCal program. Radiocarbon 37, 425–430.
Bronk Ramsey, C., 2008. Deposition models for chronological records. Quat. Sci. Rev. 27, 42–60.
Browne, E., Firestone, F.B., 1986. Table of Radioactive Isotopes (V.S. Shirley (red.). Wiley, New York.
Catalan, J., Pla-Rabes, S., Wolfe, A.P., Smol, J.P., Ruhland, K.M., Anderson, N.J.,

Kopacek, J., Stuchlık, E., Schmidt, R., Koinig, K.A., Camarero, L., Flower, R.J., Heiri, O., Kamenik, C., Korhola, A., Leavitt, P.R., Psenner, R., Renberg, I., 2013. Global change revealed by palaeolimnological records from remote lakes: a review. J. Paleolimnol. 49, 513–535.

Čechák, T., Klusoň, T., 2006. The uranium mining and storage of nuclear waste in Czech Republic. In: Čechák, T., et al. (Eds.), Nuclear Science and Safety in Europe. Springer, pp. 207–216.

Cimova, N., Novak, M., Chrastny, V., Curik, J., Veselovsky, F., Blaha, V., Prechova, E., Pasava, J., Houskova, M., Bohdalkova, L., Stepanova, M., Mikova, J., Krachler, M., Komarek, A., 2016. Lead fluxes and $^{206}Pb/^{207}Pb$ isotope ratios in rime and snow collected at remote mountain-top locations (Czech Republic, Central Europe): patterns and sources. Atmos. Environ. 143, 51–59.

Cole, K.L., Engstrom, D.R., Fytyma, R.P., Stottlemyer, R., 1990. Past atmospheric deposition of metals in northern Indiana measured in a peat core from Cowles Bog. Environ. Sci. Technol. 24 (4), 543–549.

Corker, ChJ., 2016. The Business and Technology of the Sheffield Armaments Industry 1900-1930. Doctoral. Sheffield Hallam University.

Cuddihy, R.G., Finch, G.L., Newton, G.J., Hahn, F.F., Mewhinney, J.A., Rothenberg, S.J., Powers, D.A., 1989. Characteristics of radioactive particles released from the Chernobyl nuclear reactor. Environ. Sci. Technol. 23 (1), 89–95.

De Vleeschouwer, F., Fagel, N., Cheburkin, A., Pazdur, A., Sikorski, J., Mattielli, N., Renson, V., Fialkiewicz, B., Piotrowska, N., Le Roux, G., 2009. Anthropogenic impacts in North Poland over the last 1300 years - a record of Pb, Zn, Cu, Ni and S in an ombrotrophic peat bog. Sci. Total Environ. 407–21, 5674–5684.

De Vleeschouwer, F., Le Roux, G., Shotyk, W., 2010. Peat as an archive of atmospheric pollution and environmental change: a case study of lead in Europe. PAGES News 18 (1), 20–22.

De Vleeschouwer, F., Pazdur, A., Luthers, C., Streel, M., Mauquoy, D., Wastiaux, C., Le Roux, G., Moschen, R., Blaauw, M., Pawlyta, J., Sikorski, J., Piotrowska, N., 2012. A millennial record of Environ. change in peat deposits from the Misten bog (East Belgium) Quater. Int. 268, 44–57.

Devell, L., Tovedal, H., Bergström, U., Appelgren, A., Chyssler, J., Andersson, L., 1986. Initial observations of fallout from the reactor accident at Chernobyl. Nature 321 (6067), 192–193.

Diehl, P., 2011. Uranium mining and milling wastes: an introduction. https://www.wise-uranium.org/uwai.html. (Accessed 18 May 2011).

Dolnickova, D., Drozdova, J., Raclawsky, K., Juchelkova, D., 2012. Geochemistry of trace elements in fly ashes from lignite fired power stations. J. Polish Mineral Eng. Soc. 1–6, 59–68.

Erel, Y., Axelrod, T., Veron, A., Mahrer, Y., Katsafados, P., Dayan, U., 2002. Transboundary atmospheric lead pollution. Environ. Sci. Technol. 36 (15), 3230–3233.

Erel, Y., Dayan, U., Rabi, R., Rudich, Y., Stein, M., 2006. Trans boundary transport of pollutants by atmospheric mineral dust. Environ. Sci. Technol. 40 (9), 2996–3005.

Ettler, V., Mihaljevič, M., Komárek, M., 2004. ICP-MS measurements of lead isotopic ratios in soils heavily contaminated by lead smelting: tracing the sources of pollution. Anal. Bioanal. Chem. 378 (2), 311–317.

Ettler, V., Mihaljevič, M., Šebek, O., Molek, M., Grygar, T., Zeman, J., 2006. Geochemical and Pb isotopic evidence for sources and dispersal of metal contamination in stream sediments from the mining and smelting district of Příbram, Czech Republic. Environ. Pollut. 142 (3), 409–417.

Fiałkiewicz-Kozieł, B., Smieja-Król, B., Palowski, B., 2011. Heavy metal accumulation in two peat bogs from southern Poland. Stud. Quat. 28, 17–24.

Fiałkiewicz-Kozieł, B., Kołaczek, P., Piotrowska, N., Michczyński, A., Łokas, E., Wachniew, P., Woszczyk, M., Sensuła, B., 2014. High-resolution age-depth model of a peat bog in Poland as an important basis for paleoenvironmental studies. Radiocarbon 56, 109–125.

Fiałkiewicz-Kozieł, B., Smieja-Król, B., Ostrovnaya, T.M., Frontasyeva, M., Siemińska, A., Lamentowicz, M., 2015a. Peatland microbial communities as indicators of the extreme atmospheric dust deposition. Water, air, & Soil Pollut. 226, 97–103.

Fiałkiewicz-Kozieł, B., Kołaczek, P., Michczyński, A., Piotrowska, N., 2015b. The construction of a reliable absolute chronology for the last two millennia in an anthropogenically disturbed peat bog: limitations and advantages of using a radio-isotopic proxy and age-depth modelling. Quat. Geochronol. 25, 83–95.

Fiałkiewicz-Kozieł, B., Smieja-Krol, B., Frontasyeva, M., Slowinski, M., Marcisz, K., Lapshina, E., Gilbert, D., Buttler, A., Jassey, V.E., Kaliszan, K., Laggoun-Defarge, F., Kolaczek, P., Lamentowicz, M., 2016. Anthropogenic- and natural sources of dust in peatland during the Anthropocene. Sci. Rep. 6, 38731.

Fiałkiewicz-Kozieł, B., De Vleeschouwer, F., Mattielli, N., Fagel, N., Palowski, B., Pazdur, A., Smieja-Król, B., 2018. Record of Anthropocene pollution sources of lead in disturbed peatlands from Southern Poland. Atmos. Environ. 179, 61–68.

Fleischer, R.L., Raabe, O.G., 1978. Recoiling alpha-emitting nuclei. Mechanisms for uranium-series disequilibrium. Geochem. Cosmochim. Acta 42 (7), 973–978.

Furmankiewicz, M., Krzyżanowski, K., 2008. Podziemne relikty kopalni niklu w Szklarach. Dzieje górnictwa – element europejskiego dziedzictwa kultury. In: Zagożdżon, P.P., Madziarz, M. (Eds.), Wrocław, pp. 51–60 (in Polish).

Galer, S.J.G., Abouchami, W., 1998. Practical application of lead triple spiking for correction of instrumental mass discrimination. 8th Goldschmidt Conf. Min. Mag. 62A, 491–492.

Gałka, M., Szal, M., Bruder, T., Loisel, J., Knorr, K.-H., 2019. Peatbog resilience to pollution and climate change over the past 2700 years in the Harz Mountains, Germany. Ecol. Indicat. 97, 183–193.

Gerdol, R., Degeto, S., Mazzotta, D., Vecchiati, G., 1994. The vertical distribution of the ^{137}Cs derived from Chernobyl fallout in uppermost Sphagnum layer of two peatlands in the southern Alps (Italy). Water Air Soil Pollut. 75 (1), 93–106.

Givelet, N., Le Roux, G., Cheburkin, A., Chen, B., Frank, J., Goodsite, M.E., Kempter, H., Krachel, M., Noernberg, T., Rausch, N., Rheinberger, S., Roos-Barraclough, F., Sapkota, A., Scholz, Ch, Shotyk, W., 2004. Suggested protocol for collecting, handling and preparing peat cores and peat samples for physical, chemical, mineralogical and isotopic analyses. J. Environ. Monit. 6, 481–492.

Grousset, F.E., Quetel, C.R., Thomas, B., Buatmenard, P., Donard, O.F.X., Bucher, A., 1994. 15 Transient Pb isotopic signatures in the western-european atmosphere. Environ. Sci. Technol. 28, 1605–1608.

Grübler, A., 2002. Trends in global emissions: carbon, sulphur, and nitrogen. In: Douglas, I. (Ed.), IIASA, Laxenburg, Austria, pp. 35–53.

Haack, U.K., Gutsche, F.H., Plessow, K., Heinrichs, H., 2002. On the isotopic composition of Pb in cloud waters in Central Germany. A source discrimination study. Water Air Soil Pollut. 139, 261–288.

Haack, U.K., Heinrich, H., Gutsche, F.H., Plessow, K., 2003. The isotopic composition of anthropogenic Pb in soil profiles of northern Germany: evidence for pollutant Pb from a continent-wide mixing system. Water Air Soil Pollut. 150, 113–134.

Hanslík, E., Marešová, D., Juranová, E., Sedlářová, B., 2018. Kinetics of ^{3}H, ^{90}Sr and ^{137}Cs content changes in hydrosphere in the Vltava River system (Czech Republic). J. Environ. Radioact. 188, 1–10.

Hansson, S.V., Claustres, A., Probst, A., de Vleeschouwer, F., Baron, S., Galop, D., Mazier, F., Le Roux, G., 2017. Atmospheric and Terrigenous Metal Accumulation over 3000 Years in a French Mountain Catchment: Local vs Distal Influences Anthropocene, vol. 19, pp. 45–54.

Hemming, S.R., McLennan, S.M., 2001. Pb isotope compositions of modern deep sea turbidites. Earth Planet. Sci. Lett. 184, 489–503.

Hölgye, Z., Filgas, R., 1995. Inventory of ^{238}Pu and $^{239+240}Pu$ in the soil of Czechoslovakia in 1990 journal of environmental radioactivity, 27, 181–189.

Holgye, Z., Maly, M., 2000. Sources, vertical distribution, and migration rates of 239,240Pu, 238Pu, and 137Cs in grassland soil in three localities of central Bohemia. J. Environ. Radioact. 47, 135–147.

Hölzer, A., 2010. Die Torfmoose Südwestdeutschlands und der Nachbargebiete. Weissdorn Verlag Jena, Jena 247.

Hua, Q., Barbetti, M., Rakowski, A.J., 2013. Atmospheric adiocarbon for the period 1950-2010. Radiocarbon 55, 2059–2072.

Jędrysek, M.O., Kałużny, A., Hoefs, J., 2002. S and O isotope ratios in spruce needles as a tracer of atmospheric pollution. J. Geophys. Res. Atmospheres 107, 4353–4365.

Jones, K.B., Ruppert, L.F., Swanson, S.M., 2012. Leaching of elements from bottom ash, economizer fly ash, and fly ash from two coal-fired power plants. Int. J. Coal Geol. 94, 337–348.

Kajukało, K., Fiałkiewicz-Kozieł, B., Gałka, M., Kołaczek, M., Lamentowicz, M., 2016. Abrupt ecological changes in the last 800 years inferred from a mountainous bog using testate amoebae traits and multi-proxy data. Eur. J. Protistol. 55, 165–180.

Kasztelewicz, Z., 2018. Raport o stanie branży węgla brunatnego w Polsce i w Niemczech wraz z diagnozą działań dla rozwoju tej branży w I połowie XXI wieku. www.cire.pl/pliki/2/2018/raport_o_stanie_branzy_wegla_brunatnego_w_polsce_i_w_niemczech.pdf. (Accessed 23 April 2018).

Kempter, H., Frenzel, B., 2000. The impact of early mining and smelting on the local tropospheric aerosol detected in ombrotrophic peat bogs in the Harz, Germany. Water Air Soil Pollut. 121 (1–4), 93–108.

Ketris, M.P., Yudovich, YaE., 2009. Estimations of Clarkes for Carbonaceous biolithes: world averages for trace element contents in black shales and coals. Int. J. Coal Geol. 78, 135–148.

Kicińska, A., 2019. Chemical and mineral composition of fly ashes from home furnaces, and health and environmental risk related to their presence in the environment. Chemosphere 215, 574–585.

Kolář, T., Čermák, P., Oulehle, F., Trnka, M., Štepánek, P., Cudlín, P., Hruška, J., Büntgen, U., Rybníček, M., 2015. Pollution control in the 1980 s contributed to unprecedented spruce growth in the"BlackTriangle",The Czech-Polish Border region. Sci. Total Environ. 538, 703–711.

Komarek, M., Ettler, V., Chrastny, V., Mihaljevic, M., 2008. Lead isotopes in environmental sciences: a review. Environ. Int. 34, 562–577.

Krachler, M., Shotyk, W., 2004. Natural and anthropogenic enrichments of molybdenum, thorium, and uranium in a complete peat bog profile, Jura Mountains, Switzerland. J. Environ. Monit. 6 (5), 418–426.

Krachler, M., Mohl, C., Emons, H., Shotyk, W., 2003. Atmospheric deposition of V, Cr, and Ni since the late Glacial: effects of climatic cycles, human impacts, and comparison with crustal abundances. Environ. Sci. Technol. 37, 2658.

Krajniak, W., 2017. History of the electrification of lower Silesia in the years 1891–1939. Rocznik ziem zachodnich 1, 422–461.

Laine, J., Harju, P., Timonen, T., Laine, A., Tuittila, E.-S., Minkkinen, K., Vasander, H., 2011. The intricate beauty of Sphagnum mosses — a Finnish guide to identification. Univ.Hels. Dep. For. Sci. Publ. 2, 1–191.

Lamentowicz, M., Galka, M., Milecka, K., Tobolski, K., Lamentowicz, L., Fialkiewicz-Koziel, B., Blaauw, M., 2013. A 1300-year multi-proxy, high-resolution record from a rich fen in northern Poland: reconstructing hydrology, land use and climate change. J. Quat. Sci. 28 (6), 582–594.

Le Roux, G., Hansson, S.V., Claustres, A., 2016. Inorganic Chemistry in the Mountain Critical Zone: are the mountain water towers of contemporary society under threat by trace contaminants ?. In: Mountain Ice and Water - Investigations of the Hydrologic Cycle in Alpine Environments. Developments in Earth Surface

Processes, pp. 131–154.
Mauquoy, D., van Geel, B., 2007. Mire and peat macros. In: Elias, S.A. (Ed.), Encyclopaedia of Quaternary Science, vol. 3. Elsevier Science, Amsterdam, Netherlands, pp. 2315–2336.
Mazur, S., Aleksandrowski, P., Kryza, R., Oberc-Dziedzic, T., 2006. The variscan orogen in Poland. Geol. Q. 50, 89–118.
Mazurski, K., 1986. The destruction of forests in the polish Sudetes Mountains by industrial emissions. For. Ecol. Manag. 174, 303–315.
Mietelski, J.W., Wąs, B., 1995. Plutonium from Chernobyl in Poland. Appl. Radiat. Isot. 46, 1203–1211.
Mietelski, J.W., Kubica, B., Gaca, P., Tomankiewicz, E., Błażej, S., Tuteja-Krysa, M., Stobiński, M., 2008. ^{238}Pu, $^{239+240}$Pu, ^{241}Am, ^{90}Sr and ^{137}Cs in mountain soil samples from the Tatra National Park (Poland). J. Radioanal. Nucl. Chem. 275, 523–533.
Mietelski, J.W., Kierepko, R., Łokas, E., Cwanek, A., Kleszcz, K., Tomankiewicz, Łokas, E., Mróz, T., 2016. Combined, sequential procedure for determination of ^{137}Cs, ^{40}K, ^{63}Ni, ^{90}Sr, ^{230,232} Th, ^{234,238} U, ^{237}Np, $^{238,239+240}$Pu and ^{241}Am applied for study on contamination of soils near Żarnowiec Lake (northern Poland). J. Radioanal. Nucl. Chem. 310 (2), 661–670.
Migała, K., Urban, G., Tomczyński, K., 2016. Theor. Appl. Climatol. 125, 337–351.
Mihaljevič, M., Zuna, M., Ettler, V., Šebek, O., Strnad, L., Goliáš, V., 2006. Lead fluxes, isotopic and concentration profiles in a peat deposit near a lead smelter (Příbram, Czech Republic). Sci. Total Environ. 372, 334–344.
Mihaljevič, M., Ettler, V., Strnad, L., Šebek, O., Drahota, P., Rohovec, J., 2009. Isotopic composition of lead in Czech coals. Int. J. Coal Geol. 78 (1), 38–46.
Millot, R., Allègre, C.J., Gaillardet, J., Roy, S., 2004. Lead isotopic systematics of major river sediments: a new estimate of the Pb isotopic composition of the Upper Continental Crust. Chem. Geol. 203, 75–90.
Mróz, T., Łokas, E., Kocurek, J., Gąsiorek, M., 2017. Atmospheric fallout radionuclides in peatland from Southern Poland. J. Environ. Radioact. 175–176, 25–33.
Munn, R.E., 1972. Air Quality_Local, regional and global aspects. Spec. stud 24.
Nieminen, T.M., Ukonmaanaho, L., Shotyk, W., 2002. Enrichments of Cu, Ni, Zn, Pb and as in an ombrothrophic peat bog near a Cu–Ni smelter in Southwest Finland. Sci. Total Environ. 292, 81–89.
Novak, M., Emmanuel, S., Vile, M.A., Erel, Y., Véron, A., Paces, T., Wieder, R.K., Vanecek, M., Stepanova, M., Brizova, E., Hovorka, J., 2003. Origin of lead in eight Central European peat bogs determined from isotope ratios, strenghts, and operation times of regional pollution sources. Environ. Sci. Technol. 37, 437–445.
Novak, M., Brizova, E., Adamova, M., Erbanova, L., Bottrell, S.H., 2008. Accumulation of organic carbon over the past 150 years in five freshwater peatlands in western and central Europe. Sci. Total Environ. 390 (2–3), 425–436.
OECD-IAEA, 2003. www.oecd-nea.org/ndd/pubs/2004/5291-uranium-2003.pdf.
Okamoto, S., Tanimoto, H., 2016. A review of atmospheric chemistry observations at mountain sites. Progress Earth Planet. Sci. 3, 34.
Öko-Institut, 2017. Die deutsche Braunkohlenwirtschaft - HistorischeEntwicklungen, Ressourcen, Technik, wirtschaftliche Strukturen und Umweltauswirkungen". Studie im Auftrag von Agora Energiewende und der European Climate Foundation. Berlin: Öko-Institut. https://www.agoraenergiewende.de/fileadmin/Projekte/2017/Deutsche_Braunkohlenwirtschaft/Agora_Die-deutsche-Braunkohlen-wirtschaft_WEB.pdf.
Pacyna, E.G., Pacyna, J.M., Fudala, J., Strzelecka- Jastrząb, E., Hlawiczka, S., Panasiuk, D., Nitter, S., Pregger, Th, Pheiffer, H., Friedrich, R., 2007. Current and future emissions of selected heavy metals to the atmosphere from anthropogenic sources in Europe. Atmos. Environ. 41 (38), 8557–8566.
Popowski, B., 2005. Results of a palynological analysis of peat sediments from izerskie Bagno (izerskie Mts.). Acta Botanica Silesiaca 2, 95–106.
Poręba, G., Bluszcz, A., 2007. Determination of the initial ^{137}Cs fallout on the areas contaminated by Chernobyl fallout. Geochronometria 26, 35–38.
Pratte, S., De Vleeschouwer, F., Garneau, M., 2017. Geochemical characterization (REE, Nd and Pb isotopes) of atmospheric mineral dust deposited in two maritime peat bogs from the St. Lawrence North Shore (eastern Canada). J. Quat. Sci. 32 (5), 617–627.
Procházka, R., Ettler, V., Goliáš, V., Klementová, M., Mihaljevic, M., Šebek, O., Strnad, L., 2009. A comparison of natural and experimental long-term corrosion of uranium-colored glass. J. Non-Cryst. Solids 35, 2134–2142.
Rao, R.R., Cooper, E.L., 1995. Separation of low levels of actinides by selective oxidation/reduction and co-precipitation with neodymium fluoride. J. Radioanal. Nucl. Chem. 197 (1), 133–148.
Reimer, P., Bard, E., Bayliss, A., Beck, J.W., Blackwell, P.G., Bronk Ramsey, C., Buck, C.E., Cheng, H., Edwards, R.L., Friedrich, M., Grootes, P.M., Guilderson, T.P., Haflidason, H., Hajdas, I., Hatté, C., Heaton, T.J., Hoffmann, D.L., Hogg, A.G., Hughen, K.A., Kaiser, F.K., Kromer, B., Manning, S.W., Niu, M., Reimer, R.W., Richards, D.A., Scott, M.E., Southon, J.R., Staff, R.A., Turney, C.S.M., van der Plicht, J., 2013. IntCal13 and Marine13 radiocarbon age calibration curves 0–50,000 years cal. BP. Radiocarbon 55, 1869–1887.
Rene, M., 2008. History of uranium mining in central Europe. In: Uranium Safety, Resources, Separation and Thermodynamic Calculation (Ed. Awwad N.). IntechOpen, pp. 1–20.
Rose, N.L., 2015. Spheroidal carbonaceous fly ash particles provide a globally synchronous stratigraphic marker for the Anthropocene. Environ. Sci. Technol. 49 (7), 4155–4162.
Rosen, K., Vinichuk, M., Johanson, K.J., 2009. ^{137}Cs in a raised bog in central Sweden. J. Environ. Radioact. 100, 534–539.
Le Roux, G., Fagel, N., De Vleeschouwer, F., van Leeuwen, J.F., Shotyk, W., 2012. Volcano- and climate-driven changes in atmospheric dust sources and fluxes since the Late Glacial in Central Europe. Geology 40 (4), 335–338.
Samson, P.J., 1988. Atmospheric transport and dispersion of air pollutants associated with vehicular emissions. In: Watson, A.Y., Bates, R.R., Kennedy, D. (Eds.), Air Pollution, the Automobile, and Public Health. National Academies Press (US), Washington (DC).
Sapkota, A., 2006. Mineralogical, Chemical, and Isotopic (Sr, Pb) Composition of Atmospheric Mineral Dusts in an Ombrotrophic Peat Bog, Southern South America. PhD dissertation. University of Heidelberg, p. 182.
Schwartz, M.N., Elliott, D.L., Birn, M.B., Gover, G.L., 1994. Wind Energy Resource in Poland. Pacific Northwest Laboratory Richland, Washington, pp. 1–41.
Shotyk, W., 1996. Natural and anthropogenic enrichments of As, Cu, Pb, Sb, and Zn in ombrotrophic versus minerotrophic peat bog profiles, Jura Mountains, Switzerland. Water Air Soil Pollut. 90 (3–4), 375–405.
Shotyk, W., Weiss, D., Appleby, P.G., Cheburkin, A.K., Frei, R., Gloor, M., Kramers, J.D., Reese, S., van der Knaap, W.O., 1998. History of atmospheric lead deposition since 12,370 14C yr BP from a peat bog, Jura Mountains, Switzerland. Science 281, 1635–1640.
Shotyk, W., Krachler, M., Martinez-Cortizas, A., 2002. A peat bog record of natural, pre-anthropogenic enrichments of trace elements in atmospheric aerosols since 12 370 C-14 yr BP, and their variation with Holocene climate change. Earth Planet. Sci. Lett. 199, 21–37.
Sill, C.W., 1987. Precipitation of actinides as fluorides or hydroxides for high resolution alpha spectrometry. Nucl. Chem. Waste Manag. 7, 201–215.
Skrzypek, G., Baranowska-Kacka, A., Keller-Sikora, A., Jedrysek, M.-O., 2009. Analogous trends in pollen percentages and carbon stable isotope composition of Holocene peat - possible interpretation for palaeoclimate studies. Rev. Palaeobot. Palynol. 156 (3–4), 507–518.
Smieja-Król, B., Fiałkiewicz-Kozieł, B., 2014. Quantitative determination of minerals and anthropogenic particles in some Polish peat occurrences using a novel SEM point - counting method. Environ. Monit. Assess. 186, 2573–2587.
Smieja-Król, B., Fiałkiewicz-Kozieł, B., Michalska, A., Krzykawski, T., Smołka-Danielowska, D., 2019. Deposition of mullite in peatlands of southern Poland: implications for recording large-scale industrial processes. Environ. Pollut. 250, 717–727.
Smith, A.J.E., 2004. The Moss Flora of Britain and Ireland, second ed. Cambridge University Press, Cambridge, p. 1011.
Sobik, M., Błaś, M., Migała, M., Godek, M., Nasiółkowski, T., 2014. Klimat. In: Knapik, R., Raj, A. (Eds.), Przyroda Karkonoskiego Parku Narodowego. Karkonoski Park Narodowy, Jelenia Góra, DIMOGRAF Bielsko-Biała, pp. 147–186.
Stach, A., 1996. Możliwosci i ograniczenia zastosowania cezu-137 do badan erozji gleb na obszarze Polski. Instytut Uprawy, Nawożenia i Gleboznawstwa w Puławach. Seria K 2.11, 203–226.
Strzyszcz, Z., Magiera, T., 2001. Record of industrial pollution in Polish ombrotrophic peat bogs. Phys. Chem. Earth A Solid Earth Geod. 26 (11–12), 859–866.
Szynkiewicz, A., Modelska, M., Jędrysek, M.O., Mastalerz, M., 2008. The effect of acid rain and altitude on concentration, d34S, and d18O of sulfate in the water from Sudety Mountains. Chem. Geol. 249, 36–51.
Taylor, R.N., Ishizuka, O., Michalik, A., Milton, J.A., Croudace, I.W., 2015. Evaluating the precision of Pb isotope measurement by mass spectrometry. J. Anal. Atomic Spectrom. 30 (1), 198–213.
Tyszka, R., Pietranik, A., Kierczak, J., Ettler, V., Mihaljevič, M., Weber, J., 2012. Anthropogenic and lithogenic sources of lead in lower Silesia (Southwest Poland): an isotope study of soils, basement rocks and anthropogenic materials. Appl. Geochem. 27, 1089–1100.
Ukonmaanaho, L., Nieminen, T., Rausch, N., Shotyk, W., 2004. Heavy metal and arsenic profiles in ombrogenous peat cores from four differently loaded areas in Finland. Water Air Soil Pollut. 58, 277–294.
UNSCEAR, 1982. Ionizing Radiation: Sources and Biological Effects. United Nations Scientific Committee on the Effects of Atomic Radiation, New York.
Vanneste, H., De Vleeschouwer, F., Bertrand, S., Martínez-Cortizas, A., Vanderstraeten, A., Mattielli, N., Coronato, A., Piotrowska, N., Jeandel, C., Roux, G.L., 2016. Elevated dust deposition in Tierra del Fuego (Chile) resulting from Neoglacial Darwin Cordillera glacier fluctuations. J. Quat. Sci. 31 (7), 713–722.
Vassilev, S.V., Greta, M., Eskenazy, G.M., Vassileva, C.G., 2001. Behaviour of elements and minerals during preparation and combustion of the Pernik coal, Bulgaria. Fuel Process. Technol. 72, 103–129.
Veron, A., Novak, M., Brizova, E., Stepanova, M., 2014. Environmental imprints of climate changes and anthropogenic activities in the Ore Mountains of Bohemia (Central Europe) since 13 cal. kyr BP. Holocene 24 (8), 919–931.
Vile, M.A., Wieder, R.K., Novak, M., 2000. 200 years of Pb deposition throughout the Czech republic: patterns and sources. Environ. Sci. Technol. 34, 12–21.
Vrablik, P., Wildova, E., Vrablikova, J., 2017. The effect of Brown coal mining on the environment and health of the population in northern bohemia (Czech republic). Int. J. Clean Coal Energy 6 (1), 1–13.
Wardenaar, E.P.C., 1987. A new hand tool for cutting peat profiles. Can. J. Bot. 65, 1772–1773.
Waters, C.N., Zalasiewicz, J., Summerhayes, C., Fairchild, I.J., Rose, N., Loader, N.J., Shotyk, W., Cearreta, A., Head, M.J., Syvitski, J.P.M., Williams, M., Wagreich, M., Barnosky, A.D., Zhisheng, A., Leinfelder, R., Jeandel, C., Gałuszka, A., IvardoSul, J.A., Gradstein, F., Steffen, W., McNeill, J.R., Wing, S., Poirier, C., Edgeworth, M., 2018. Global boundary stratotype section and point (GSSP) for the anthropocene series: where and how to look for potential candidates. Earth Sci. Rev. 178, 379–429.

Waters, C.N., Zalasiewicz, J., Summerhayes, C., Barnosky, A.D., Poirier, C., Gałuszka, A., Cearreta, A., Edgeworth, M., Ellis, E.C., Ellis, M., Jeandel, C., Leinfelder, R., McNeill, J.R., Richter, D. de B., Steffen, W., Syvitski, J., Vidas, D., Wagreich, M., Williams, M., Zhisheng, An, Grinevald, J., Odada, E., Oreskes, N., Wolfe, A.P., 2016. The Anthropocene is functionally and stratigraphically distinct from the Holocene. Science 351, 137.

Wedepohl, K.H., 1995. The composition of the continental crust. Geochem. Cosmochim. Acta 59 (7), 1217–1232.

Weis, D., Kieffer, B., Maerschalk, C., Pretorius, W., Barling, J., 2005. High-precision Pb-Sr-Nd Hf isotopic characterization of USGS BHVO-1 and BHVO-2 reference materials: comparison of first and second generation samples. Geochem. Geophys. Geosyst. 6.

Weiss, D., Shotyk, W., Kramers, J.D., Gloor, M., 1999. Sphagnum mosses as archives of recent and past atmospheric lead deposition in Switzerland. Atmos. Environ. 33, 3751–3763.

Wolkersdorfer, Ch, 1995. Die Flutung des ehemaligen Uranbergwerks Niederschlema/Alberoda der SDAG Wismut Z. geol. Wiss. 23 (5/6), 795–808.

Yafa, C., Farmer, J.G., Graham, M.C., Bacon, J.R., Barbante, C., Cairns, W.R.L., Bindler, R., Renberg, I., Cheburkin, A., Emons, H., Handley, M.J., Norton, S.A., Krachler, M., Shotyk, W., Li, X.D., Martinez-Cortizas, A., Pulford, I.D., MacIver, V., Schweyer, J., Steinnes, E., Sjøbakk, T.E., Weiss, D., Dolgopolova, A., Kylander, M., 2004. Development of an ombrotrophic peat bog (low ash) reference material for the determination of elemental concentrations. J. Environ. Monitor. 6, 493–501.

Yang, H., Rose, N.L., Boyle, J.F., Battarbee, R.W., 2001. Storage and distribution of trace metals and spheroidal carbonaceous particles (SCPs) from atmospheric deposition in the catchment peats of Lochnagar, Scotland. Environ. Pollut. 115, 231–238.

Yao, P.H., Shyu, G.S., Chang, Y.F., Chou, Y.C., Shen, C.C., Chou, C.S., Chang, T.K., 2015. Lead isotope characterization of petroleum fuels in Taipei, Taiwan. Int. J. Environ. Res. Public Health 4602–4616.

Zimmermann, F., Bothmer, D., 2000. Die Emissions situation im Schwarzen Dreieck, gestern-heute-morgen. In: Final report of project OMKAS, 15–22, Ed.: Sächsisches Landesamt für Umwelt und Geologie,Zur Wetterwarte 11, D-01109 Dresden, Germany.

Zuna, M., Mihaljevič, M., Šebek, O., Ettler, V., Handley, M., Navrátil, T., Goliáš, V., 2011. Recent lead deposition trends in the Czech Republic as recorded by peat bogs and tree rings. Atmos. Environ. 45 (28), 4950–4958.

Łokas, E., Mietelski, J.W., Kleszcz, K., Tomankiewicz, E., 2010. A sequential procedure for determining ^{238}Pu, $^{239+240}$Pu, ^{241}Am, ^{90}Sr, U and Th activities in soils and peats from Spitsbergen. Nukleonika 55, 195–199.

Łokas, E., Mietelski, J.W., Ketterer, M.E., Kleszcz, K., Wachniew, P., Michalska, S., Miecznik, M., 2013. Sources and vertical distribution of ^{137}Cs, ^{238}Pu, $^{239+240}$Pu and ^{241}Am in peat profiles from southwest Spitsbergen. Appl. Geochem. 28, 100–108.

Łukaszek-Chmielewska, A., Stawarz, O., Isajenko, K., Piotrowska, B., Girard, M., 2018. Radiological assessment of radionuclide contents in soils in Lower Silesian Voivodeship in the years 1988-2014. Web of Conferences 45, 00048.